Mathematical Biosciences and Engineering

https://www.aimspress.com/journal/mbe

MBE, 23(11): 3436–3469.
DOI: 10.3934/mbe.2026118
Received: 01 July 2026
Revised: 11 October 2026
Accepted: 19 October 2026
Published: 18 November 2026

Research article

A multiscale statistical analysis of the relationship between climate variability and dengue incidence in Mexico

Inder Tecuapetla-Gómez[1], Héctor De la Torre Gutiérrez[2], Mayra Núñez-López[3,*] and L. Leticia Ramírez-Ramírez[4,*]

[1] Secretaría de Ciencia, Humanidades, Tecnología e Innovación-Comisión Nacional para el Conocimiento y Uso de la Biodiversidad, Insurgentes Sur 4903, Mexico City 14010, Mexico

[2] Secretaría de Ciencia, Humanidades, Tecnología e Innovación-Centro de Investigación en Matemáticas, Cal de la Plenitud 103, Aguascalientes 20200, Mexico

[3] Department of Mathematics, Instituto Tecnológico Autónomo de México, Río Hondo 1, Ciudad de México 01080, Mexico

[4] Probability and Statistics, Centro de Investigación en Matemáticas, Jalisco S/N, Guanajuato 36023, Mexico

* **Correspondence:** Email: mayra.nunez@itam.mx, leticia.ramirez@cimat.mx.

Abstract: Dengue transmission in Mexico exhibits substantial spatial and temporal variability driven by climatic and environmental conditions. We investigated the relationship between climate variability and weekly dengue incidence using epidemiological, demographic, geographic, and environmental data from 2475 municipalities between 2011 and 2021. A multiscale statistical framework was developed by integrating national scale models (NSMs) and local scale models (LSMs). At the national level, generalized linear and Bayesian hierarchical spatial models were evaluated under different probability distributions, lag structures, and random-effect specifications. Municipality-level Bayesian models were subsequently used to characterize local transmission dynamics. National analyses showed that climatic covariates, together with municipality-level heterogeneity, explained a large proportion of the observed variation in dengue incidence. In contrast, local models revealed considerable regional differences in the contribution of individual climatic predictors, indicating that climate–dengue relationships are spatially heterogeneous. Moreover, shorter lag structures generally improved non-spatial models, whereas longer lags were more competitive in spatial models. These findings highlight the importance of integrating national and local analyses to better characterize dengue transmission and support geographically targeted surveillance and control strategies.

Keywords: dengue; climate variability; multiscale modeling; Bayesian hierarchical models

1. Introduction

Dengue is one of the most important vector-borne viral diseases worldwide, affecting more than 120 countries and causing an estimated 390 million infections annually [1, 2]. Its rapid expansion over recent decades has been driven by a combination of urbanization, human mobility, environmental change, and the geographic spread of *Aedes aegypti*, the primary mosquito vector of the disease. Because dengue transmission depends on vector ecology, climatic conditions play a central role in determining where and when outbreaks occur. Temperature, precipitation, and humidity influence mosquito survival, larval development, biting frequency, and the duration of the virus extrinsic incubation period [3, 4]. Recent studies further confirm that climatic suitability remains a key determinant of dengue expansion across tropical and subtropical regions [5, 6].

Numerous studies have shown that climatic variability affects dengue transmission through nonlinear and delayed mechanisms, as moderate increases in temperature may accelerate mosquito development and viral replication, while precipitation modulates the availability of breeding sites and may generate effects with lags of some weeks [7, 8]. Climate anomalies associated with large-scale phenomena such as *El Niño* have also been linked to substantial increases in dengue incidence in Latin America and Southeast Asia [9, 10]. Early time series and climate disease studies established that temperature and precipitation are major drivers of dengue dynamics [7, 11], while subsequent global and regional analyses confirmed that transmission is constrained by thermal and ecological suitability, shaping both seasonal patterns and long-term geographic limits [1, 12, 13].

These advances have motivated the development of statistical and spatiotemporal models that integrate environmental information with epidemiological surveillance data. Bayesian hierarchical models, spatiotemporal frameworks, and forecasting-oriented approaches have improved the characterization of transmission patterns and the anticipation of dengue outbreaks [14–18]. However, most studies have focused either on broad national or regional analyses aimed at describing large-scale trends, or on local investigations restricted to specific endemic areas. Nevertheless, few studies have examined whether the relationship between climatic covariates and dengue incidence remains consistent across spatial scales within the same country.

This distinction is particularly relevant in geographically heterogeneous countries such as Mexico, where dengue transmission occurs across regions with markedly different climatic, environmental, and demographic conditions. Some regions experience persistently high dengue transmission, whereas others differ in climate, population density, and local environmental conditions, resulting in marked differences in disease incidence. As a result, national analyses may identify broad climatic associations but mask local heterogeneity, whereas local analyses may reveal regional mechanisms that are not apparent after spatial aggregation. Understanding how these two levels of analysis complement each other is therefore essential for interpreting dengue dynamics and for informing surveillance strategies.

In this study, we analyze the relationship between climatic variables and weekly dengue incidence at the municipal level in Mexico using official epidemiological surveillance data and environmental covariates. Municipal-level dengue case data were obtained through a direct request to the General Directorate of Epidemiology of the Mexican Ministry of Health, allowing us to examine spatiotemporal transmission patterns over the period 2011–2021. The considered climatic variables are temperature, precipitation, evaporation, and elevation, together with spatial and temporal components that account for municipal heterogeneity and seasonal variation.

The analysis is organized through a multiscale statistical framework that combines two complementary model classes. First, national scale models (NSMs) are used to study dengue transmission across all municipalities of Mexico within a common modeling structure. These models provide a broad view of spatial and temporal patterns, allowing the identification of large-scale associations between climatic variability, geographic heterogeneity, and dengue incidence. Second, local scale models (LSMs) are used to examine selected municipalities and their surrounding regions at a finer spatial scale. These models examine dengue transmission at the local level, providing information that complements the national analysis.

By combining national and local statistical models, this study provides a comprehensive assessment of the relationship between climate and dengue incidence across spatial scales in Mexico. Rather than viewing national and local analyses as alternative approaches, we show that they provide complementary information. National models identify broad climatic patterns associated with dengue transmission, whereas local models reveal regional differences that become less apparent after spatial aggregation. Together, these analyses provide a more complete understanding of how climatic factors influence dengue dynamics and illustrate the importance of considering spatial scale when interpreting epidemiological relationships.

The remainder of the paper first describes the climatic and epidemiological data used in the analysis (Sections 2 and 3) before presenting the multiscale modeling framework (Section 4) and the corresponding national and municipal level results (Section 5). Section 6 discusses the results and future work.

2. Climatic drivers of dengue incidence

Dengue transmission is strongly influenced by environmental conditions that affect mosquito abundance, vector competence, and human–vector contact. Climatic variables therefore provide measurable indicators of the ecological conditions associated with disease transmission and have been linked to dengue risk across a wide range of geographic and temporal scales. In this study, we considered four environmental covariates: weekly mean temperature, weekly precipitation, weekly evaporation, and mean municipal elevation. These variables represent both short-term climatic variability and broader geographic characteristics that are relevant to dengue transmission.

- *Temperature* is one of the main environmental determinants of dengue transmission. It influences *Aedes aegypti* survival, development rates, biting frequency, and the extrinsic incubation period of the virus. Transmission tends to increase under intermediate temperatures, roughly between 20 and 30 °C, whereas very low or high temperatures reduce mosquito survival and transmission efficiency [19].
- *Precipitation* contributes to the formation of breeding sites through the accumulation of standing water in natural and artificial containers. Its influence is often nonlinear and delayed, reflecting mosquito development and viral incubation processes. Moderate and intermittent rainfall is frequently associated with increased dengue transmission, particularly in urban environments [20].
- *Evaporation* reflects atmospheric water demand and integrates the effects of temperature, humidity, radiation, and wind. Although high evaporation may reduce the persistence of outdoor breeding sites, it can also coincide with heat conditions that promote household water storage and container-based breeding. For this reason, evaporation provides complementary information on

moisture dynamics and climatic stress not fully captured by precipitation alone [11, 20].

- *Elevation* represents a relatively stable geographic characteristic. Higher elevations are generally associated with lower temperatures and greater thermal variability, conditions that limit mosquito survival and viral replication. As a consequence, elevation serves as a useful proxy for long-term ecological constraints on sustained dengue transmission in regions with complex topography such as Mexico [12, 13].

3. Data

3.1. Municipalities and population

The municipality is the basic unit of this analysis and comprises 2475 municipalities (including the boroughs of Mexico City). Their geographic information was obtained from the Geostatistical Framework of the National Institute of Statistics and Geography (INEGI) (https://www.inegi.org.mx/temas/mg/), while population data were retrieved from the mid-annual population estimates produced by the National Population Council, CONAPO [21]. These annual population estimates are based on the General Census of Population and Housing, and Figure 1 shows the logarithms of total population by municipality according to the Population and Housing Census conducted in 2020 by the INEGI.

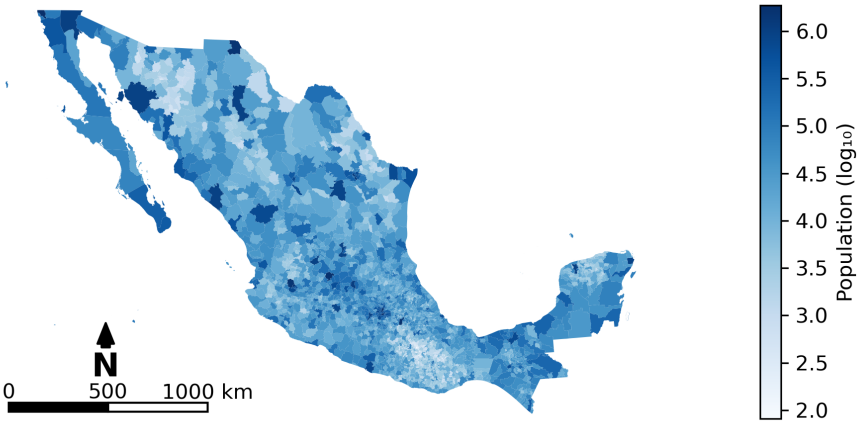


Figure 1. Map of Mexico that displays the logarithm of the population in each municipality, according to the Population and Housing Census 2020, INEGI. Source: https://www.inegi.org.mx/programas/ccpv/2020/#datos_abiertos.

3.2. Spatial data and neighborhood structure

Municipal polygons are used to represent the spatial structure of Mexico. The municipal shapefile is reprojected to the *Mexico ITRF2008 / Lambert Conformal Conic* coordinate reference system (EPSG: 6372), which has been the official coordinate reference system used by the INEGI for topographic mapping and area calculations across Mexico [22].

3.3. Dengue

Weekly confirmed dengue cases are accesible for each municipality from epidemiological week 1 of 2011 through epidemiological week 52 of 2021. In Mexico, the first epidemiological week of 2011 began on Sunday, January 2, 2011, which coincides with the first week of the ISO calendar (ISO 8601), which defines weeks as starting on Sunday. Figure 2 depicts this data that was obtained through a direct request to the General Directorate of Epidemiology of the Mexican Ministry of Health (https://www.gob.mx/salud/acciones-y-programas/direccion-general-de-epidemiologia).

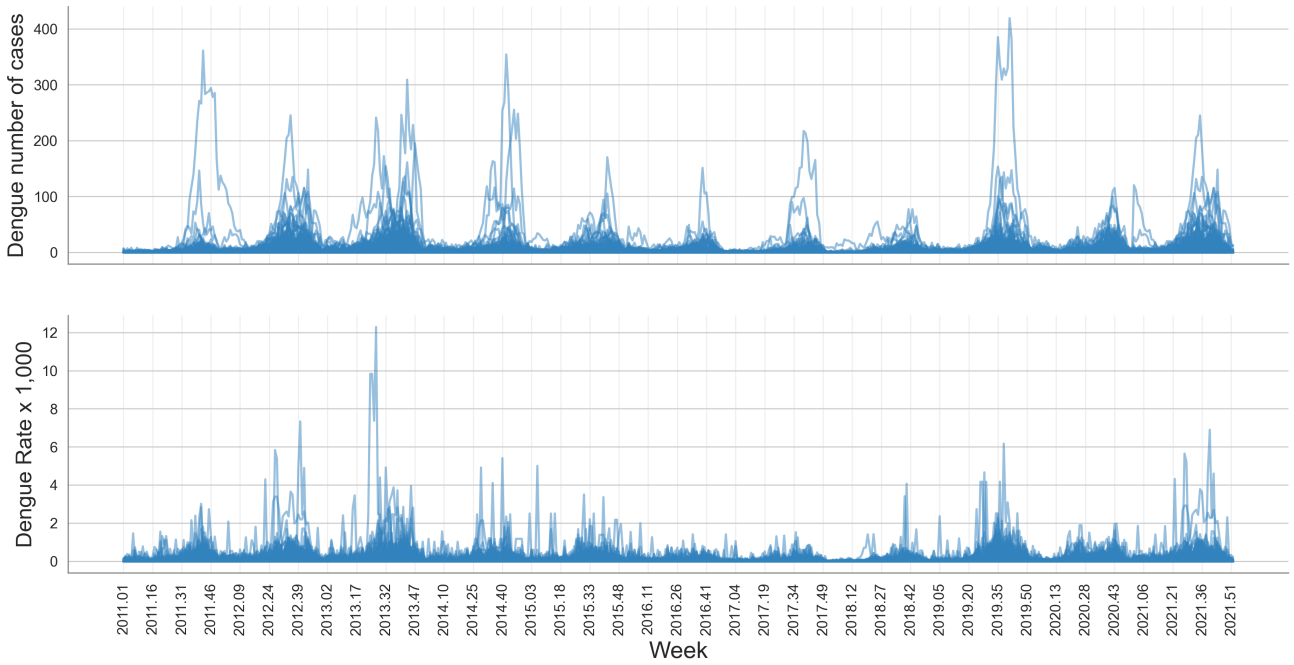


Figure 2. Weekly dengue number of cases and rate (per 1000 people) by municipality for the period 2011–2021. Source: General Directorate of Epidemiology of the Mexican Ministry of Health: https://www.gob.mx/salud/acciones-y-programas/direccion-general-de-epidemiologia.

3.4. Elevation

Elevation above sea level was obtained from the INEGI layer "Mexican Elevation Continuum and Digital Elevation Models" (Version 4.0, at 15 meters of spatial resolution), available at https://www.inegi.org.mx/app/geo2/elevacionesmex/. Figure 3 shows the average elevation for each municipality, which is used as a covariate in the statistical models.

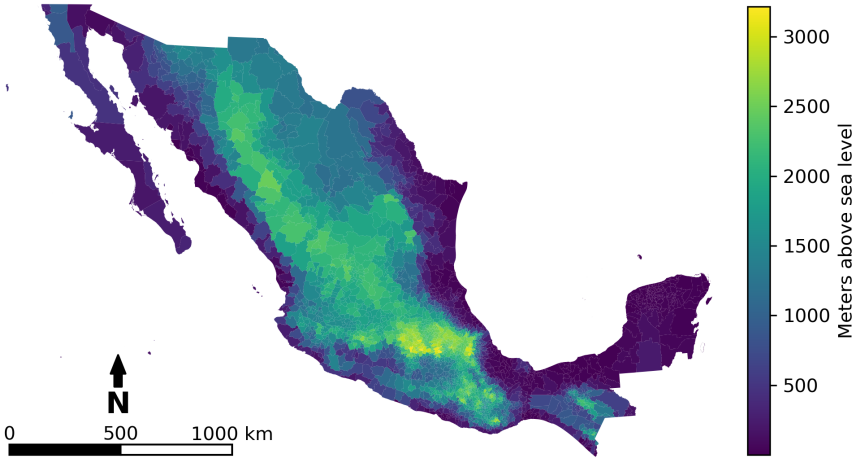


Figure 3. Average municipal elevation in meters above sea level. Source: Mexican Elevation Continuum and Digital Elevation Models, INEGI. https://www.inegi.org.mx/app/geo2/elevacionesmex/.

3.5. Temperature, precipitation, and evaporation

Weekly temperature, precipitation, and evaporation data were obtained from the ERA5-Land reanalysis dataset [23], produced by the European Center for Medium-Range Weather Forecasts (ECMWF) [24]. ERA5-Land variables were extracted at a spatial resolution of 0.1° (~ 9 km at the equator). Temperature, originally acquired in Kelvin, was converted to degrees Celsius (°C) by subtracting 273.15. Precipitation and evaporation are expressed as meters of water equivalent (m), representing accumulated depths over the chosen time step (e.g., daily totals), whereas temperature is instantaneous at 2 m above the surface.

Temperature corresponds to the estimated instantaneous air temperature at 2 meters above the land surface; precipitation represents total accumulated precipitation (rain, snow, and other hydrometeors) at the surface; and evaporation corresponds to total surface evaporation, including evaporation, transpiration, and sublimation fluxes and accumulations.

Although these products are available at an hourly temporal resolution and extend back to January 1950, weekly composites were generated for this study beginning in the first week of January 2011. Weekly mean temperature was computed as the arithmetic average of hourly values, while weekly precipitation and evaporation were computed by first aggregating daily totals and subsequently calculating weekly averages.

This procedure yielded 1293 raster layers corresponding to the period from the first week of 2001 through week 45 of 2025. Each raster layer is a matrix of 204 rows and 353 columns, resulting in a total of 72,012 georeferenced cells (pixels) covering the Mexican territory.

In order to obtain representative temperature, precipitation, and evaporation values for each municipality, we calculated area-weighted means from gridded raster data. Specifically, for every raster cell intersecting a polygon, the cell value was multiplied by the fraction of its area contained within the polygon. The weighted sum was then normalized by the total intersected area. This approach ensures that each cell contributes proportionally to its spatial coverage, avoiding biases from partial

overlaps. Area-weighted averaging is the recommended method for aggregating intensive variables such as temperature, precipitation, and evaporation from gridded datasets to irregular administrative units [25, 26]. It has been widely applied in climatology, hydrology, and ecological modeling to derive spatially consistent statistics from raster data [27–29].

National-level time series for the climatic variables were downloaded using the Google Earth Engine platform [30]. Figure 4 illustrates the temporal variability of temperature, precipitation, and evaporation through weekly means and interquartile ranges during 2011–2025. These series reveal marked seasonal patterns together with substantial interannual variability across Mexico.

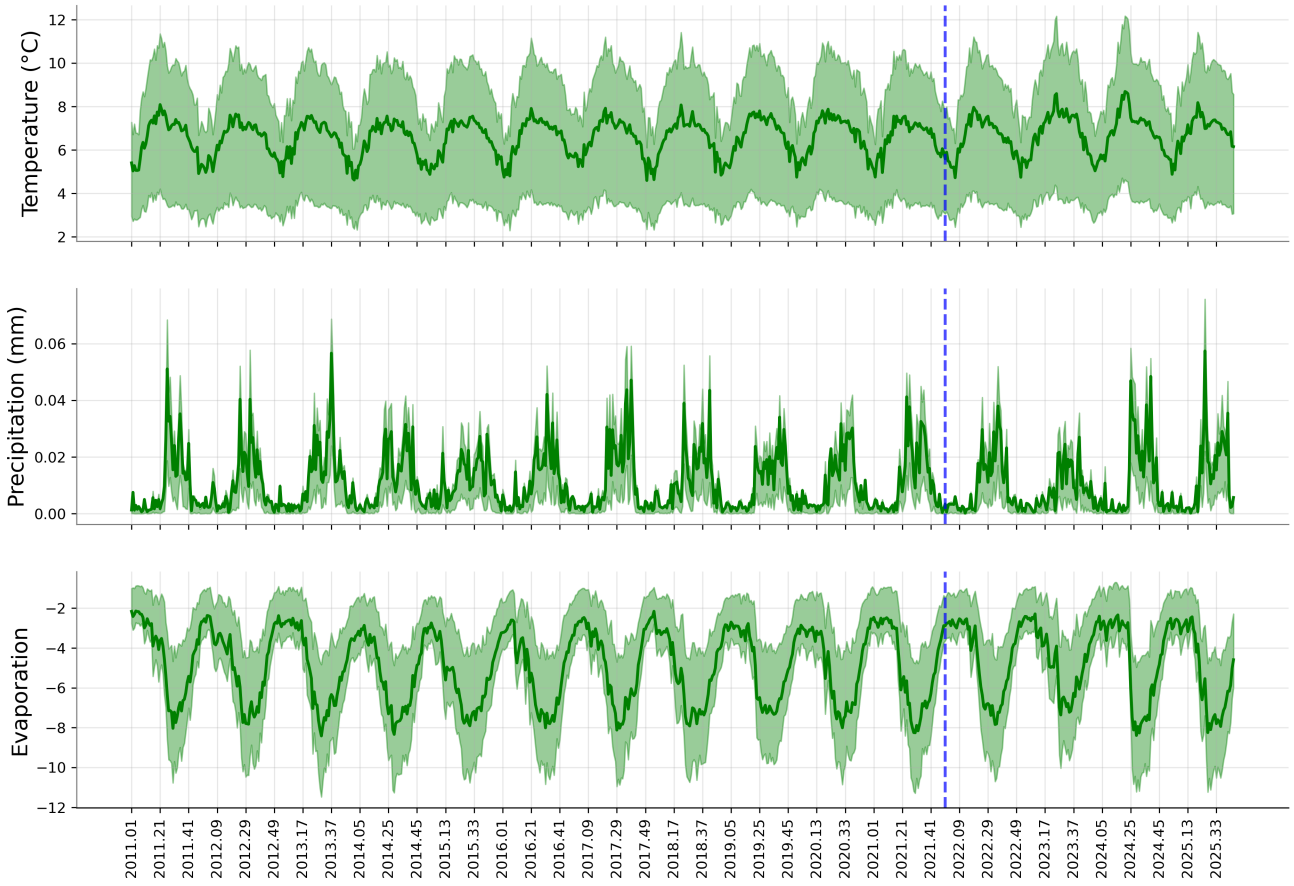


Figure 4. Weekly environmental variables: mean (green lines) and interquartile range (green shaded areas) of the municipality series (2011–2025). The blue dashed lines indicate the series from 2011 to 2021.

The consolidated database consists of the number of confirmed dengue cases (y_{it}), elevation (elev_{it}), population (pop_{it}), temperature (temp_{it}), precipitation (precip_{it}), and evaporation (evap_{it}), where i is any of the 2475 municipalities and t is any of the 572 weeks in the 2011–2021 period. Notice that $\text{elev}_{it} \equiv \text{elev}_i$ and $\text{pop}_{i,t_1} = \text{pop}_{i,t_2}$ for t_1 and t_2 in the same calendar year. The resulting database contains a total of 1,415,700 rows and integrates epidemiological, climatic, demographic, and geographic information at the municipal level across Mexico. This dataset provides the basis for examining the relationship between climatic variability and dengue incidence, and motivates the modeling framework presented in the following section.

3.6. Some notation and covariate transformations

The one-to four-week lag window was selected based on the biological timing of dengue transmission. Under the temperature conditions commonly observed in dengue-endemic regions of Mexico (approximately 25–30 °C), the immature stages of *Aedes aegypti* (egg, larva, and pupa) require about 7–10 days to develop into adults, whereas a blood-fed female completes a gonotrophic cycle in approximately 3–4 days [3, 4]. After a mosquito becomes infected by feeding on an infectious human, the virus requires an additional 5–15 days to complete the extrinsic incubation period and reach the salivary glands, depending on temperature [31]. In humans, the intrinsic incubation period before symptom onset is typically 4–7 days [31]. These successive processes suggest that changes in temperature or precipitation are unlikely to affect reported dengue cases immediately. Instead, their effect is expected to appear after approximately two to four weeks, once mosquito development, viral incubation, human incubation, and reporting delays are taken into account. This time scale is consistent with previous studies relating climate variability to dengue transmission. For example, analyses in Mexico have reported significant associations between climatic anomalies and dengue incidence over several weeks [10], while studies in Puerto Rico found the strongest cumulative effects of temperature and precipitation during the current and following months [7]. Based on this biological and empirical evidence, we evaluated lag values of $\ell = 1, 2, 3$, and 4 weeks for temperature, precipitation, and evaporation. Longer lag structures were not considered because they are more likely to introduce multicollinearity among the climatic variables. Next, we present the covariate transformations common to both the NSMs and LSMs.

Lagged environmental covariates

Because the effect of climatic variables on dengue transmission is not immediate, lagged versions of evaporation, temperature, and precipitation are generated for lags of one to four weeks. For municipality i and week t, the lagged variables are defined as:

$$\begin{aligned} \text{evap}_{i,t-\ell} &= \text{evap_}\ell_{it}, \\ \text{temp}_{i,t-\ell} &= \text{temp_}\ell_{it}, \\ \text{precip}_{i,t-\ell} &= \text{precip_}\ell_{it}, \end{aligned}$$

where $\ell = 0, 1, 2, 3, 4$ denotes the lag in weeks, with $\ell = 0$ corresponding to the original covariate.

Lagged covariates are included in the analysis using either separate-lag or joint-lag models. For instance, for separated lags, instead of including lags 1–4 simultaneously in the same model, four sets of models were fitted independently: one using lag 1 covariates, one using lag 2 covariates, one using lag 3 covariates, and one using lag 4 covariates. This strategy reduced multicollinearity among highly correlated lagged meteorological variables and allowed comparison of predictive performance across different lag windows.

Time-invariant or nearly weekly time-invariant municipal-level variables (elevation and population) are not lagged.

Covariate standardization

All continuous covariates are standardized using the mean and standard deviation calculated exclu-

sively from the training data. For a covariate $\boldsymbol{x}$, the standardized variable is defined as:

$$z_x = \frac{\boldsymbol{x} - \bar{x}}{s_{\boldsymbol{x}}}, \tag{3.1}$$

where $\bar{x}$ and $s_{\boldsymbol{x}}$ are the training-set mean and standard deviation, respectively.

For any lag $\ell = 0, 1, 2, 3, 4$, the models include the following standardized covariates: z_{elev}, $z_{\text{evap_}\ell}$, $z_{\text{temp_}\ell}$, and $z_{\text{precip_}\ell}$.

4. Methods

To properly account for the dengue incidence, including other characteristics such as overdispersion and spatial dependence, we employ generalized linear models (GLMs) [32] or generalized linear mixed models (GLMMs) [33], where the response variable, y_{it}, is the weekly count of dengue cases. The use of generalized linear models (GLMs) and generalized linear mixed models (GLMMs) becomes highly convenient as not only do GLMMs offer a natural and parsimonious framework for handling the hierarchical and correlated nature of the data, but GLMs with negative binomial or zero-inflated specifications directly address overdispersion and possible excess zeros. Also, by incorporating random intercepts at the municipality and year levels, GLMMs can also explicitly account for unobserved municipal heterogeneity and within-municipal serial correlation without the need to estimate a large number of fixed-effect parameters.

In general, the considered GLMMs have the expression:

$$g(\mathbb{E}(\boldsymbol{y})) = \mathbf{X}\boldsymbol{\beta} + \mathbf{Z}\mathbf{u}, \tag{4.1}$$

where $g(\cdot)$ is a *link* function, $\mathbb{E}(\boldsymbol{y})$ denotes the expected value of the variable of interest, $\mathbf{X}$ is the design matrix with the covariates, $\boldsymbol{\beta}$ is the fixed-effects regression coefficients, $\mathbf{Z}$ is the design matrix for the random effects, and $\mathbf{u}$ is a vector of the random effects.

The GLMMs considered in this work can be understood as a natural extension of the generalized linear models (GLMs) [34, 35]. While a standard GLM relates the expected value of the response to a linear combination of covariates through a link function, $g(\mathbb{E}(y)) = \mathbf{X}\boldsymbol{\beta}$, it assumes that all observations are independent conditional on the fixed effects alone, and therefore does not explicitly account for correlation arising from spatial, temporal, or hierarchical structure in the data. The GLMM extends this formulation by incorporating additional random effects [33]. In Eq (4.1), the term $\mathbf{X}\boldsymbol{\beta}$ retains the same role as in the GLM, capturing the fixed effects of the observed covariates, while $\mathbf{Z}\mathbf{u}$ introduces a set of random effects $\mathbf{u}$, typically assumed to follow a specified distribution (e.g., Gaussian), which allow the model to account for unobserved heterogeneity, correlation between observations, and structured dependence, such as that induced by spatial factors and the quality of measurements. In this sense, the GLM can be viewed as a special case of the GLMM in which the random-effects design matrix $\mathbf{Z}$ is absent (or $\mathbf{u} = \mathbf{0}$), and the GLMM generalizes this framework by allowing the mean structure to depend on both fixed and random components, while still preserving the flexibility of the link function $g(\cdot)$ to accommodate non-Gaussian response distributions, such as those appropriate for count data like dengue case counts.

All studied models in this work use the logarithm as the link function and a population log-offset that accounts for exposure to dengue cases relative to each municipality's total population. The logarithmic

link function was used because it is the canonical and most commonly adopted link function for GLMs applied to count data [34, 35]. The log link provides a natural way to relate the expected number of cases to the linear predictor while ensuring that the fitted mean remains positive. A population log-offset, which accounts for exposure to dengue cases relative to each municipality's total population, is introduced:

$$\log\left(\frac{\mathbb{E}(y_{it})}{\text{pop}_{it}}\right) = \log(\mathbb{E}(y_{it})) - \log(\text{pop}_{it}) = \mathbf{X}\boldsymbol{\beta} + \mathbf{Zu}.$$

Therefore, the models estimate relative dengue incidence rates rather than absolute counts. Now, this model is extended so that the right-hand-side elements can incorporate spatial and temporal information as both fixed and random effects.

In this study, we employed the model given by Eq (4.1), explicitly accounting for spatiotemporal structure:

$$\log(\mathbb{E}(y_{it})) = \log(\text{pop}_{it}) + f_{it} + (z_\ell_{it})^{\top}\,\boldsymbol{\beta} + b_{it} + S_i, + T_t, \tag{4.2}$$

where pop_{it} is the population in municipality i at week t, f_{it} represents a municipality-time-dependent trend, the vector z_ℓ_{it} contains fixed effects based on combinations of predictors (including lagged transformations), the term b_{it} captures random effects, while S_i denotes the spatially structured component designed to reflect influences from neighboring municipalities, and T_t represents a time-dependent process of order p.

To describe the heterogeneity in the dengue incidence that cannot be explained by the spatiotemporal structure, three different distributions for y_{it} are considered:

1) Poisson: $y_{it} \sim \text{Poisson}(\mu_{it})$.
2) Negative binomial model (NB): $y_{it} \sim \text{NB}(\mu_{it}, \kappa)$.
3) Zero-inflated Poisson model (ZIP):

$$y_{it} \sim \begin{cases} 0, & \text{with probability } \pi, \\ \text{Poisson}(\mu_{it}), & \text{with probability } 1-\pi, \end{cases} \tag{4.3}$$

where π is the probability of an excess zero.

The first model derives directly from the standard Poisson model. Here, y_{it} is assumed to follow a Poisson distribution with mean μ_{it}, and this model restricts the variance of y_{it} to be equal to its mean. To relax this assumption and allow for more realistic scenarios, we consider the negative binomial model, which has the capacity to describe count data whose variance exceeds its mean (a scenario known as overdispersion). In the context of epidemiological surveillance, and in particular for dengue counts, some municipalities experienced considerably larger counts during outbreak periods. This pattern may lead to extra-Poisson variability that the standard Poisson model cannot accommodate.

Another common characteristic of reports or measurements collected from natural phenomena is a high frequency of reported zeros. While distributions such as the Poisson and negative binomial can also produce zeros, an excess of zeros may indicate the presence of an additional data-generating mechanism that "inflates" the frequency of this value. For instance, a municipality may report no dengue cases not because transmission was truly absent, but because of a shortage in testing capacity or personnel during that period. To account for these excess zeros, "zero-inflated" versions of a distribution consider two distinct data-generating processes: one producing structural zeros (e.g., due to

a lab or reporting shortage) and another producing counts from the underlying distribution (including genuine zero dengue cases in the municipality) [35,36]. These two processes are incorporated through a mixture parameter π, as shown in (4.3): y_{it} is equal to zero either because it is a structural zero, with probability π, or because it is a zero arising from the Poisson (or negative binomial) component, with probability $(1-\pi)$.

The following subsections discuss each component in detail, emphasizing its role in describing dengue incidence dynamics and highlighting the computational challenges inherent in model fitting.

4.1. National scale models (NSMs)

NSMs include different model specifications by combining alternative covariates and model components. All of the derived models are implemented using integrated nested Laplace approximation (INLA), and a final assessment is based on the best fit.

Given the scale of the national dataset, classical Markov chain Monte Carlo (MCMC) methods for statistical inference become computationally prohibitive, especially when accounting for overdispersion, hierarchical structure, municipal heterogeneity, and temporal dependence. INLA [37,38] offers a compelling solution by providing fast and accurate Bayesian inference for latent Gaussian models without the long run times and sampling inefficiencies that MCMC methods can easily present at this scale.

INLA inherently supports GLMs and GLMMs, and is particularly effective for fitting hierarchical models with spatial effects and structured temporal components. Additionally, INLA's ability to account for spatial autocorrelation through customized neighborhood matrices, such as those used in Besag and Besag-York-Mollié type 2 (BYM2) models [39], is particularly relevant. In this study, the spatial effect was represented through a BYM2 structure, while the temporal effect was represented through a second-order random walk (RW2). These components were evaluated with the remaining random effects included in the model specifications.

This framework facilitates the comparison of alternative hierarchical formulations aimed at capturing spatial dependence, unstructured heterogeneity, and smooth temporal variation. In this context, the BYM2 effect borrows strength from neighboring municipalities, whereas the RW2 effect captures changes across consecutive time periods.

Further details on the BYM2 and RW2 components of the INLA model used, as well as on the covariates included as fixed and random effects, are presented next.

In this study, all NSMs use the separated lag models (one for each lag $\ell = 1, 2, 3, 4$) and components as defined in (4.2). This is:

$$\log(\mathbb{E}(y_{it})) = \log(\text{pop}_{it}) + f_{it} + (\boldsymbol{z}_\ell_{it})^{\top}\,\boldsymbol{\beta} + b_{it} + S_i, \tag{4.4}$$

Regarding the random effect component b_{it}, four scenarios are considered. Let u_i and v_y represent a municipality-specific random intercept and a year-specific random intercept, respectively. The scenarios for b_{it} are:

1) No random effects (GLM):

$$b_{it} = 0.$$

2) Municipality-level random intercept:

$$b_{it} = u_i, \quad u_i \sim \mathcal{N}(0, \sigma_u^2). \tag{4.5}$$

3) Year-level random intercept:

$$b_{it} = v_y, \quad v_y \sim \mathcal{N}(0, \sigma_v^2). \tag{4.6}$$

4) Both municipality and year-level random intercepts:

$$b_{it} = u_i + v_y. \tag{4.7}$$

Equation (4.4) also incorporates a spatial term (S_i) and a seasonal structure (f_{it}) (via the BYM2 and RW2 components, respectively) to assess whether neighboring municipalities share residual transmission patterns beyond those explained by the observed covariates. On the one hand, INLA can include a Besag-York-Mollié type (BYM2) component that allows one to account for a municipal (purely spatial) effect and an unstructured Gaussian random effect. In this NSM model, we consider Eq (4.2) with S_i following a BYM2 model, which provides a general framework for spatial autocorrelation in the areal data. For spatial object i (municipality), the predictor S_i can be written as:

$$S_i = \alpha + \sqrt{\frac{\phi}{\tau}}\, u_i + \sqrt{\frac{1-\phi}{\tau}}\, v_i, \tag{4.8}$$

where α is an overall intercept, τ is the overall precision (inverse variance), and $\phi \in [0, 1]$ is the mixing parameter, representing the proportion of variance explained by the structured component.

Additionally,

$$u_i \mid u_{-i} \sim \mathcal{N}\left(\frac{1}{n_i}\sum_{j\in\partial_i} u_j, \frac{1}{n_i}\right) \quad \text{and} \quad v_i \sim \mathcal{N}(0, 1), \tag{4.9}$$

where ∂_i and n_i denote the set and number of neighbors of municipality i, respectively. Thus, the vector $\boldsymbol{u} = (u_1, \ldots, u_n)$ follows the so-called intrinsic conditional autoregressive (ICAR) Gaussian prior, while the term v_i is an independent Gaussian noise. That is, the BYM2 component explicitly models the structured (spatial) and unstructured (random effects) variability.

On the other hand, to simultaneously account for residual spatial dependence and smooth temporal variation, INLA can combine the BYM2 municipal effect with a second-order random walk temporal effect (RW2). This is the term f_{it} in (4.4) and in this case, the RW2 prior assumes smooth temporal evolution and penalizes deviations from linear trends over time. That is, we let $f_{it} = \Phi_t$, and we assume

$$\Delta^2\Phi_t = (\Phi_t - \Phi_{t-1}) - (\Phi_{t-1} - \Phi_{t-2}) = \Phi_t - 2\Phi_{t-1} + \Phi_{t-2} \sim \mathcal{N}(0, \tau_\Phi^{-1}), \tag{4.10}$$

where τ_Φ is the temporal precision parameter.

These extended models should be interpreted cautiously because BYM2 already contains an unstructured municipal component; therefore, the additional municipal effect may introduce redundancy or identifiability issues.

In summary, based on the proposed model specifications of Eq (4.4), this study evaluates whether the inclusion of spatial and temporal components, random effects at different hierarchical levels, lagged covariates, and alternative probability distributions for y_{it} improves the predictive performance for the total number of dengue cases. We use the 2001–2020 data to evaluate the prediction performance for the weeks in 2021. A total of 144 model specifications are fitted with this objective.

4.2. Local scale models (LSMs)

We employed the R package brms [40–42] to fit Bayesian regression models using Hamiltonian Monte Carlo (HMC), a Markov chain Monte Carlo method that provides asymptotically exact uncertainty quantification for variance components such as municipality-level random effects, temporal correlation parameters, and overdispersion, without relying on unimodality assumptions. The flexibility of brms allows hierarchical modeling, accommodates non-Gaussian likelihoods, and enables direct specification of complex correlation structures, making it particularly well-suited for dengue surveillance data, which are characterized by overdispersion, temporal dependence, and spatial heterogeneity. Throughout this study, independently of the model specification, we employed brms with 4 chains, each with 8000 iterations and 4000 warm-ups to ensure convergence of the Markov chains.

Municipal model with HMC

In this section, in addition to the fixed effects b_{it} defined as in (4.7), the local model (4.2) incorporates three additional components. First, exploratory analysis at the municipal level suggested an underlying trend in the number of incidences, markedly during the second semester of each year (July–December), see Figure 5. To account for this behavior, we consider municipal and season-specific trends. That is, we consider the annual trend function

$$f_{it} = \Phi_i(t, s_t, w_t),$$

where $\Phi_i(\cdot, s_t, w_t)$ is a spline depending on the predictor *week index* stratified by semester each year; s_t is an indicator function that takes a value of 0 for weeks that are within the first semester, and 1 otherwise; and w_t denotes a year factor.

Second, we consider the proper conditional autoregressive (CAR) Gaussian model to account for the spatial random effect u_i conditioned on its neighbors:

$$u_i \mid u_{-i} \sim \mathcal{N}\left(\frac{\rho}{n_i}\sum_{j\in\partial_i} u_j, \frac{\sigma_u^2}{n_i}\right). \tag{4.11}$$

As in (4.9), this expression considers a weighted average of the n_i neighbors ∂_i of the municipality i, but also includes two other parameters: the spatial correlation and variance parameters ρ and σ_u^2, respectively.

Furthermore, here, the spatial component S_i in (4.2) is a special case of (4.8) that assumes $\phi = 1$, resulting in

$$S_i = \alpha + \frac{1}{\sqrt{\tau}}\, u_i,$$

with u_i defined as in (4.11) and where all variability is spatially structured. In this case, the autocorrelation parameter ρ determines the strength of dependence between neighboring areas, while τ controls the overall precision, i.e., the inverse of the variance.

The CAR structure acts as a regularizing prior on the municipality-level random effects. During estimation, each municipality's deviation from the global mean is shrunk toward the average of its neighbors, with the amount of shrinkage controlled by ρ. The parameter ρ is the global spatial autocorrelation coefficient in the CAR prior. It does not vary by edge or municipality; instead, it scales the entire adjacency matrix. A value near zero indicates that municipalities behave independently, while

a value close to one indicates strong spatial dependence, meaning each municipality's effect is heavily influenced by its neighbors. Thus, in practice, CAR reduces variance in the random effects, improves predictive fit, and ensures that the posterior distribution reflects spatial clustering rather than treating municipalities as independent units.

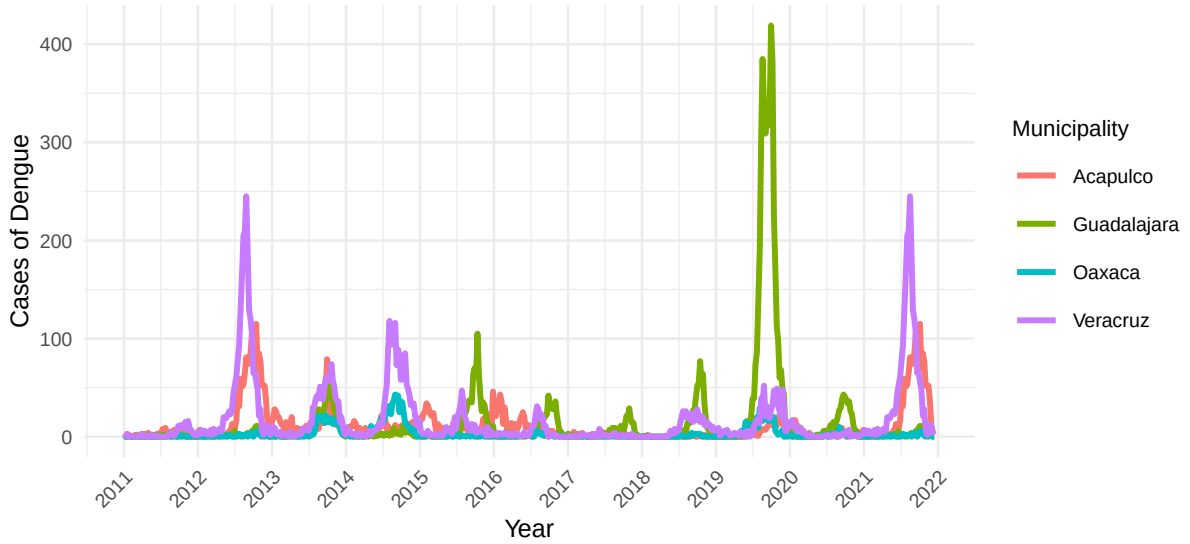


Figure 5. Dengue weekly case incidence during 2011–2021 in Acapulco, Guadalajara, Oaxaca, and Veracruz.

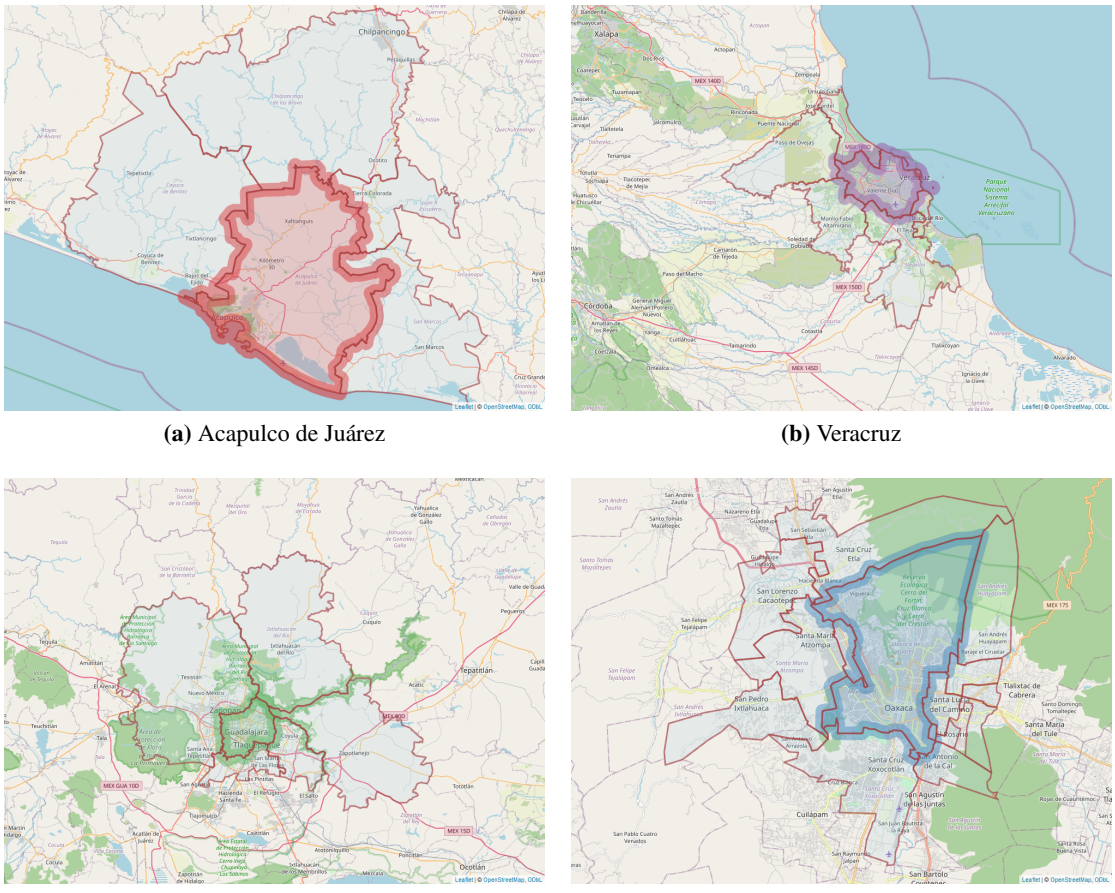
The third feature that we explore at the municipal level consists of including an autoregressive process of order 2 to try and model a possible temporal dependence. More precisely, we consider the component T_t in Eq (4.2) given by $T_t = \phi_1 T_{t-1} + \phi_2 T_{t-2} + \epsilon_t$, where $\epsilon_t \sim \mathcal{N}(0, \sigma_T^2)$.

To capture local heterogeneity in dengue dynamics, we selected four municipalities across Mexico: Acapulco on the South Pacific coast, Veracruz along the Gulf of Mexico, Guadalajara in central Mexico near the Pacific, and Oaxaca in the south. For each focal site, we defined a neighborhood consisting of its nearest surrounding municipalities within a 1-km buffer (Figure 6). Acapulco's neighborhood includes Chilpancingo, Coyuca de Benítez, San Marcos, and Juan R. Escudero. Guadalajara is bordered by Ixtlahuacán del Río to the north, Zapopan to the west, San Pedro Tlaquepaque to the south, Tonalá to the southeast, and Zapotlanejo to the east. Veracruz is surrounded by La Antigua, Paso de Ovejas, Manlio Fabio Altamirano, Medellín de Bravo, and Boca del Río. Oaxaca de Juárez is embedded in a dense municipal network, with neighbors including San Pablo Etla, San Lorenzo Cacaotepec, Santa María Atzompa, San Pedro Ixtlahuaca, San Jacinto Amilpas, Santa Cruz Xoxocotlán, San Antonio de la Cal, San Sebastián Tutla, Santa Lucía del Camino, San Agustín Yatareni, and San Andrés Huayápam. Notably, Oaxaca is situated within the state that contains the largest number of municipalities in Mexico (570), underscoring the complexity of its administrative and spatial structure.

The municipality-level analysis complements the national analysis by exploring dengue transmission within distinct epidemiological settings. Whereas national models identify broad climatic and spatial patterns, local models help assess how these relationships vary across regions.

We note that all fitted models, GLMMs and INLA-based national models, as well as the CAR-based local models, assume a log-linear relationship between climatic covariates and expected dengue incidence. This specification captures monotonic associations but does not allow for the unimodal,

threshold-type responses that are biologically expected for temperature (e.g., transmission peaking within an intermediate thermal range and declining at both low and high extremes). Consequently, the reported coefficients and incidence rate radios (IRRs) should be interpreted as average linear associations over the observed range of each covariate rather than as a full characterization of the underlying dose-response relationship. Future extensions of this framework could incorporate nonlinear terms (e.g., splines or quadratic terms) for the climatic covariates, analogous to the splines already used here to capture seasonal trends in the local models.



(a) Acapulco de Juárez **(b)** Veracruz

(c) Guadalajara **(d)** Oaxaca

Figure 6. Geographic location of the municipalities included in the study areas. This contextual figure illustrates the spatial positioning of the selected municipalities and supports the description of the methodological framework.

5. Results

5.1. National scale models (NSMs)

Model evaluation

NSM performance was assessed using a temporal validation strategy. The year 2021 was reserved as the validation set, while all other years were used for model fitting. Let $\mathcal{D}_{\text{train}}$ denote the training set

and $\mathcal{D}_{\text{test}}$ the validation set:

$$\mathcal{D}_{\text{train}} = \{(i,t) : \texttt{year} \neq 2021\}, \tag{5.1}$$

$$\mathcal{D}_{\text{test}} = \{(i,t) : \texttt{year} = 2021\}. \tag{5.2}$$

GLMs and GLMMs are fitted on $\mathcal{D}_{\text{train}}$ and predictions were generated for $\mathcal{D}_{\text{test}}$. For INLA-based models with temporal random effects, observations from 2021 were retained in the dataset but their response values were set to missing, allowing out-of-sample prediction for the validation period.

Some of the following metrics were used to evaluate both the fit and the predictive performance of the models:

Let y_{it} and $\hat{y}_{it}$ be the observed and fitted/predicted dengue counts for the test period (with T weeks), respectively, and the following metrics were calculated to evaluate the model's predictive performance for each municipality i:

- Root mean squared error: RMSE = $\sqrt{\sum_{t=1}^{T}(y_{it} - \hat{y}_{it})^2/n}$.
- Mean absolute error: MAE = $\sum_{t=1}^{T} |y_{it} - \hat{y}_{it}|/T$.
- Correlation between observed and predicted counts: $r = \text{cor}(y_{it}, \hat{y}_{it})$.
- Poisson deviance: $D = 2\sum_{t=1}^{T} \left[y_{it} \log\left(y_{it}/\hat{y}_{it}\right) - (y_{it} - \hat{y}_{it})\right]$.

For frequentist models, the Akaike information criterion (AIC) was reported. For INLA models, the deviance information criterion (DIC) and the widely applicable information criterion (WAIC, also known as the Watanabe-Akaike information criterion) were reported. The primary selection criterion was out-of-sample (year 2021) predictive performance, particularly lower RMSE and MAE, higher correlation, and lower Poisson deviance.

In summary, for the NSMs, the GLMs and GLMMs with regular random effects and BYM2 and BYM2 + RW2 components add up to 144 different models:

- 3 model type: GLMM, INLA + BYM2, and INLA + BYM2 + RW2.
- 3 distribution for y_{it}: Poisson, NB, and ZIP.
- 4 scenarios for covariates, according to lag ℓ: $\ell = 1, 2, 3, 4$.
- 4 different random effects b_{it}: $b_{it} = 0$, (4.5), (4.6), and (4.7).

Model scoring results

The national models showed that climatic variables together with municipality-level differences explain much of the observed variation in dengue incidence across Mexico (see Table S1). Overall, models incorporating municipality-level heterogeneity consistently outperformed simpler specifications, indicating that persistent differences among municipalities explain a substantial fraction of the observed variability in dengue incidence.

Among the eight best-performing models, Poisson models generally outperformed zero-inflated formulations, suggesting that a separation between disease-free and transmission-prone municipalities does not well-describe dengue transmission. On the other hand, spatial INLA models provided only limited improvement and the good performance of the national GLM Poisson model with municipality-level random effects suggests that broad dengue patterns across Mexico are largely captured by climatic covariates together with persistent differences among municipalities not explicitly represented in the model.

Regarding the spatial models fitted with INLA, those assuming a negative binomial distribution achieved the best performance. Within this group, the best-fitting models were those without random effects, followed by models including a municipality-level random effect. These models generally incorporated longer lag structures, particularly lags 3 and 4.

In contrast, the models that simultaneously incorporated BYM2 and RW2 random effects with longer lag structures, particularly lag 4, showed the poorest overall fit. This suggests that delayed climatic effects, represented through lagged environmental covariates, already capture an important component of temporal variability in dengue transmission, reducing the additional contribution of the RW2 temporal effect.

Overall, the ZIP distribution performed the worst among the evaluated probability distributions. For the GLM models, the Poisson distribution combined with shorter lags yielded the best results. By contrast, for the spatial models fitted with INLA, the negative binomial distribution combined with longer lag structures provided the best model fit.

The two selected models represent complementary approaches to dengue prediction. The first model was a Poisson generalized linear mixed model including municipality-level random effects and climatic covariates lagged by one week ("GLM Poisson + municipality iid, lag 1"). This model quantifies the association between climate and dengue incidence while allowing each municipality to have its own baseline risk level. The second model was an INLA BYM2 negative binomial model with climatic covariates lagged by four weeks ("INLA + BYM2 NB, lag 4"). This model additionally accounts for overdispersion and residual spatial dependence among neighboring municipalities. Together, these models distinguish the contribution of short-term climatic variation from persistent local and spatial heterogeneity in dengue risk.

Table 1. Fixed-effect estimates and incidence rate ratios for the two selected dengue models.

Model	Covariate	Estimate	SE/SD	95% interval	IRR	IRR 95% interval
GLM+Poisson + lag1	Temperature lag 1	0.1865	0.0066	[0.1735, 0.1995]	1.2051	[1.1895, 1.2208]
	Precipitation lag 1	0.0580	0.0013	[0.0554, 0.0606]	1.0597	[1.0569, 1.0625]
	Evaporation lag 1	-0.4264	0.0022	[−0.4307, −0.4220]	0.6529	[0.6500, 0.6557]
	Elevation	-1.8088	0.0483	[−1.9035, −1.7141]	0.1639	[0.1490, 0.1801]
INLA + BYM2 NB, lag4	Temperature lag 4	0.1155	0.0093	[0.0972, 0.1338]	1.1224	[1.1021, 1.1432]
	Precipitation lag 4	0.0804	0.0041	[0.0723, 0.0884]	1.0837	[1.0750, 1.0925]
	Evaporation lag 4	-0.6434	0.0061	[−0.6553, −0.6316]	0.5255	[0.5193, 0.5318]
	Elevation	-1.3647	0.0155	[−1.3950, −1.3343]	0.2555	[0.2478, 0.2633]

Note: IRR denotes that incidence rate ratio, computed as $\exp(\beta)$. IRR values greater than one indicate an increase in expected dengue incidence, whereas IRR values below one indicate a decrease in expected incidence, conditional on the remaining covariates and random effects.

Table 1 reports the fixed-effect estimates and incidence rate ratios (IRRs) for the two selected models. For the Poisson mixed model, intervals correspond to 95% confidence intervals, whereas for the INLA BYM2 negative binomial model, they correspond to 95% posterior credible intervals. In both models, the reported intervals for the covariates exclude zero on the coefficient scale and the corresponding IRR intervals exclude one, indicating consistent evidence of an association between the climatic/environmental predictors and dengue incidence, conditional on the remaining covariates and model-specific random effects. Temperature and precipitation showed positive associations with dengue incidence in both selected models. In the "GLM Poisson + municipality iid, lag 1" model, the IRR for temperature lag 1 was 1.205, while the IRR for precipitation lag 1 was 1.060. In the "INLA +

BYM2 NB, lag4" model, temperature lag 4 and precipitation lag 4 also showed positive associations, with posterior IRR values of 1.122 and 1.084, respectively. These results support the interpretation that short-term climatic variation contributes to changes in dengue incidence. Evaporation and elevation showed negative associations with dengue incidence in both models. The IRR for evaporation was 0.653 in the first model and 0.526 in the second, while elevation had IRR values of 0.164 and 0.256, respectively. These results suggest that environmental gradients contribute to differences in dengue risk, even after accounting for model-specific random effects. However, the magnitudes of the municipality-level random effects (reported in Table 2) provide evidence that dengue incidence is not explained by climatic variation alone.

Table 2. Random-effect and spatial-structure summaries for the two selected dengue models.

"GLM Poisson + municipality iid, lag 1"			
Component	Mean/estimate	95% interval	Interpretation
Municipal random-intercept variance	3.5476	–	Between-municipality heterogeneity in baseline dengue risk
Municipal random-intercept SD	1.8835	–	Log-scale variability in the municipal random intercept
exp(SD)	6.5765	–	Approximate multiplicative heterogeneity associated with one SD of the municipal random effect
"INLA + BYM2 NB, lag 4"			
Component	Mean/estimate	95% interval	Interpretation
Spatial precision / variance	0.3687	[0.3346, 0.4062]	Residual spatial component estimated by the BYM2 model
BYM2 mixing parameter	0.8544	[0.7976, 0.8969]	Large relative contribution of spatially structured variation
Negative binomial overdispersion	0.1792	[0.1772, 0.1813]	Extra-Poisson variability in dengue counts

Note: The BYM2 mixing parameter describes the relative contribution of spatially structured variation to the residual random effect. Larger values indicate a stronger contribution of spatially structured residual variation.

Table 2 summarizes the random effect and spatial structure components of both models. The "GLM Poisson + municipality iid, lag 1" model estimated a municipal random-intercept variance of 3.548 and standard deviation of 1.884 on the log scale. On the multiplicative scale, this corresponds to exp(1.8835) = 6.5765. Therefore, a one-standard-deviation difference in the municipal random intercept is associated with an approximately 6.6-fold multiplicative difference in the baseline expected dengue incidence, after accounting for the climatic covariates included in the model. This result is central to the interpretation of municipality-level heterogeneity. It indicates that municipalities differed strongly in their baseline dengue risk, even after adjustment for temperature, precipitation, evaporation, and elevation. Also, such heterogeneity may reflect unmeasured local characteristics, including demographic structure, urbanization, housing conditions, vector-control activities, health-service access, reporting practices, human mobility, and additional environmental conditions not explicitly included in the models.

Model temporal validation

The "INLA + BYM2 NB, lag 4" model provides complementary evidence by separating residual variation into spatially structured and unstructured components. Table 2 shows that the BYM2 mixing parameter had a posterior mean of 0.854 with a 95% credible interval of [0.7976, 0.8969], suggesting that a large component of the residual random variation was spatially structured. This implies that neighboring municipalities tended to share similar unexplained dengue risk patterns after adjustment

for the climatic covariates. The negative binomial overdispersion parameter was 0.179 with a 95% credible interval of [0.1772, 0.1813] (Table 2), further supporting the need to account for extra-Poisson variation in dengue counts.

Figure 7 presents two scatter plots summarizing the predictive performance of the two best-performing models in the 2021 validation set ("GLM Poisson + municipality iid, lag 1" and "INLA + BYM2 NB, lag 4"). In each panel, the points correspond to observed dengue case counts for municipality-level observations. Observations are displayed according to their predicted values, which facilitates comparison with observed counts, fitted values, and predictive uncertainty across the range of estimated risk. The color of each point indicates whether the observed dengue count was contained within the corresponding 95% prediction interval. These intervals are built as quantile intervals of the set of predicted values of dengue counts under their corresponding models, across municipalities and weeks. Points in pink are classified as inside the prediction interval (built around the predicted number of cases). For these, the model adequately captured the observed number of cases within its predictive uncertainty. In contrast, points in cyan are outside the prediction interval, indicating either underestimation or overestimation beyond the uncertainty accounted for by the model. Together, these plots provide a visual comparison of predictive calibration for the two selected models. In addition to showing how closely predicted values track observed dengue counts, the figure also highlights the extent to which each model provides realistic uncertainty bounds. A model with a larger proportion of points inside the prediction interval can be interpreted as having better prediction interval coverage, whereas a greater number of points outside the interval suggests limitations in its ability to represent the variability of dengue incidence across municipalities.

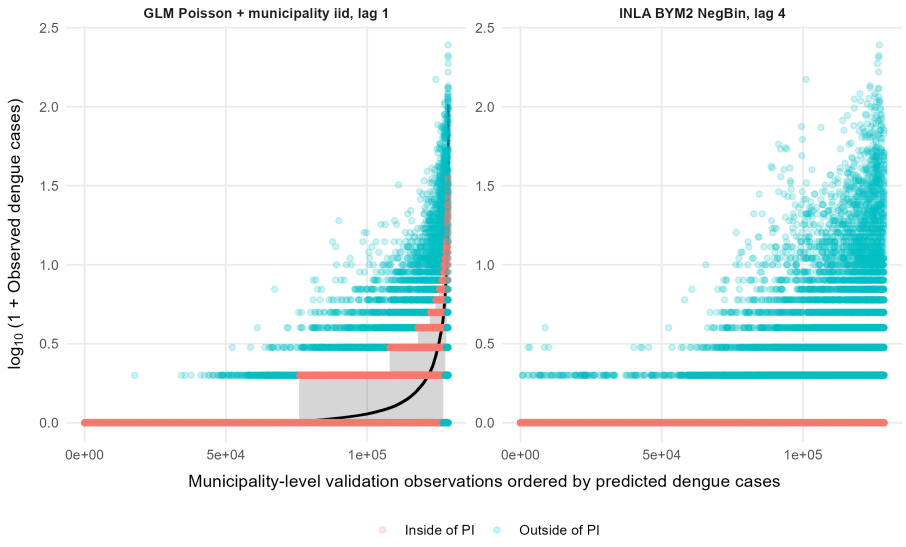


Figure 7. Municipality-week $\log_{10}(1 + \text{observed})$ vs. predicted counts in the validation set in 2021. The shaded grey area corresponds to the prediction intervals, and the paired data are colored according to whether they fall within or outside the resulting intervals.

Figure 8 summarizes the weekly coverage of the 95% prediction intervals produced by each model. That is, for each week and each model, the point represents the percentage of observed dengue cases falling within the corresponding 95% prediction interval, across a population of 2475 municipalities.

The figure shows that both models achieve coverage higher than the nominal 95% for at least one-third of the weeks in 2021; however, coverage can drop to values as low as 93% for the "GLM Poisson + municipality iid, lag 1" model and 80% for the "INLA + BYM2 NB, lag 4" model.

It is worth noting that both models may be considered suitable for short-term prediction after studying municipality or regional coverage performance. However, the one-year validation presented here is intended only to assess the models' general performance and to serve as an alternative criterion for comparing their relative performance against one another.

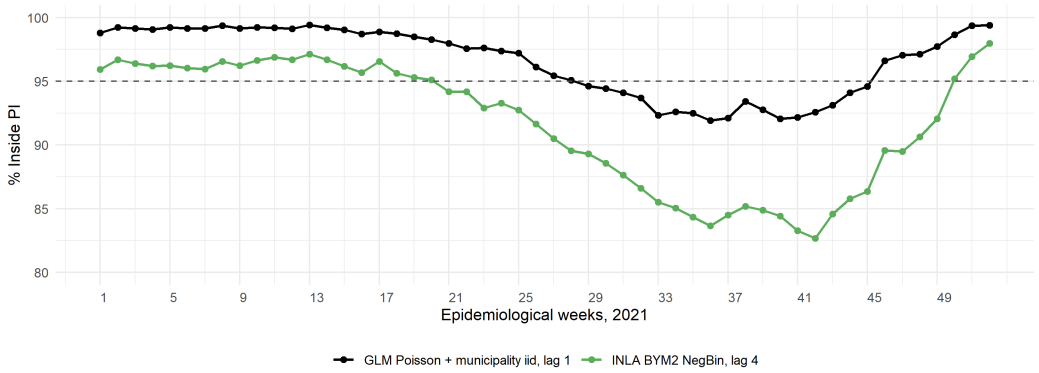


Figure 8. Weekly coverage (%) of the 95% prediction intervals for observed municipality-level dengue cases for 2021.

Now we consider examining the predictive error in terms of their spatial distribution. The INLA BYM2 negative binomial model incorporates both spatial dependence and overdispersion, so its intervals are expected to provide better coverage. A higher number of observations inside the prediction interval would indicate that this model better represents the uncertainty in dengue counts across municipalities and weeks. Observations outside the interval remain informative, as they may highlight local outbreaks, reporting anomalies, or missing environmental or socio-demographic predictors.

In Figure 9, the spatial distribution of prediction errors for the 2021 validation year is shown for the same two models. The depicted errors for each municipality were computed as the signed error for the total predicted and observed cases in the 52 weeks (as "Total observed cases - total predicted cases" corresponding to the observed-predicted headings in Figure 9). Therefore, positive values indicate underprediction (the model predicted fewer cases than were observed) and negative values indicate overprediction. For the GLM Poisson model with municipality-level random effects and a one-week lag, the error map suggests a tendency to underpredict dengue cases. A predominance of positive errors across municipalities reflects this. Such behavior is consistent with the limitations of the Poisson assumption, particularly when dengue counts exhibit overdispersion or outbreak-like behavior. In contrast, the INLA BYM2 NB model with a four-week lag tends to overpredict the number of dengue cases, as indicated by a greater presence of negative errors. The tendency toward overprediction may indicate that the spatial smoothing component distributes risk across neighboring municipalities, increasing predicted counts in areas where the observed number of cases was lower.

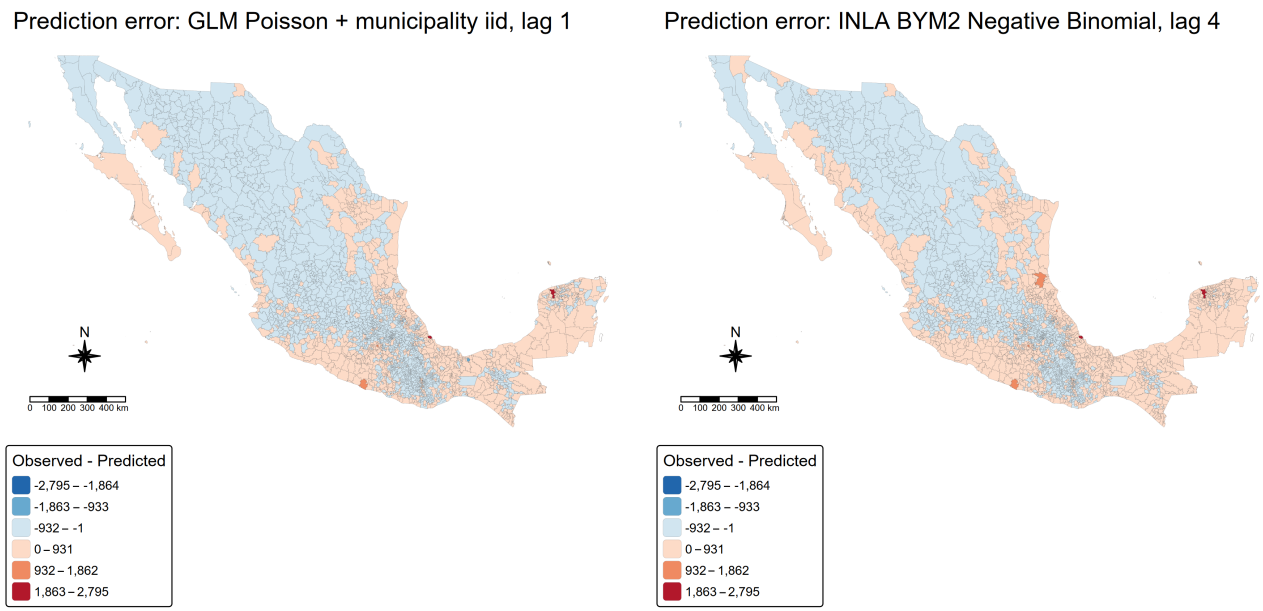


Figure 9. Municipality-signed error for the total dengue predictions in 2021.

Relative to the lag-structure comparison, shorter lags, particularly one to two weeks, tended to perform better in non-spatial models, whereas longer lags were more competitive in the spatial INLA formulations. This distinction may reflect different temporal scales through which climate influences dengue transmission. Short lags may capture more immediate ecological forcing, including recent rainfall, moisture availability, and rapid changes in vector activity. In contrast, longer lags may reflect mosquito development and subsequent transmission processes such as viral incubation and the gradual propagation of transmission across neighboring municipalities. From this perspective, the differing lag structures are not contradictory but instead suggest that climatic forcing operates across multiple temporal scales.

Figure 9 highlight differences between the two approaches. The GLM Poisson model tended to underpredict large outbreaks, whereas the spatial INLA BYM2 model often spread risk across neighboring municipalities and occasionally overpredicted low-incidence areas. These results suggest that the models capture different spatial patterns of dengue transmission.

Table 3. Predictive performance of the two selected national models in the 2021 validation set.

Model	RMSE	MAE	Correlation	Mean error	Total observed	Outside PI (n)
"GLM Poisson + municipality iid, lag 1"	3.0247	0.4680	0.4518	0.1342	53,001	4357
"INLA + BYM2 NB, lag 4"	3.4114	0.4118	0.2161	0.4118	53,001	10,699

Note: Mean error is observed minus predicted dengue cases; positive values indicate underprediction. Inside PI (n) is the number of validation observations for which the observed count fell within the model-based 95% prediction interval.

Table 3 summarizes the predictive metrics for both models during the 2021 out-of-sample validation year. The GLM Poisson model achieved a lower RMSE (3.025 vs. 3.411) and a higher observed-predicted correlation (0.452 vs. 0.216) than the BYM2 model, consistent with the GLM Poisson model attaining the best point-prediction fit among all 144 fitted national models (Table S1). However, the

BYM2 model achieved a lower MAE (0.412 vs. 0.468) and, more importantly, a substantially lower prediction-interval coverage at the weekly municipality-level. Its number of observations that fell outside the 95% prediction interval was 10,699, and that under the BYM2 model was of only 4357. This pattern indicates that the GLM Poisson model produces more accurate point predictions on average and is capable of producing better predictions.

Public health implications

From a public health perspective, the explored models and, more precisely, the two selected ones, confirm that, at the national level, the considered fixed-effect variables: temperature, precipitation, evaporation, and elevation, have a statistically significant relation with the number of dengue cases. Moreover, both fitted models agree on the direction of every covariate's effect: temperature and precipitation increase expected dengue incidence (at lags 1 or 4), while evaporation and elevation decrease it. That consistency across two fairly different model specifications (different likelihood, different random-effects structure, different lag) is itself useful evidence that these are genuine, non-spurious ecological drivers rather than artifacts of one particular model choice.

Operationally, the superior predictive performance of the GLM Poisson model further suggests that recent climatic information, through the fixed-effect estimates in Table 1, could support a first short-term surveillance tool. Because the linear predictor takes the form (4.4) with $b_{it}, S_i = 0$ and $\ell = 1$, the term f_{it} reduces to a fixed intercept β_0, and $b_{it} = u_i$ is the independent and identically distributed (iid) municipality random intercept. That is, (4.4) takes the form:

$$\log(\mu_{it}) = \log(\text{pop}_{it}) + \beta_0 + [z_{\text{temp_1}}]_{it}\,\beta_1 + [z_{\text{precip_1}}]_{it}\,\beta_2 + [z_{\text{evap_1}}]_{it}\,\beta_3 + [z_{\text{elev}}]_{it}\,\beta_4 + u_i, \tag{5.3}$$

with

$$y_{it} \mid b_i \;\sim\; \text{Poisson}(\mu_{it}) \quad \text{and} \quad u_i \overset{iid}{\sim} \mathcal{N}(0, \sigma_b^2),$$

where $\mu_{it} = \mathbb{E}(y_{it}|u_i)$ is the mean conditional to the random intercept and the z's are the observations of the standardized covariates.

Exponentiating the fixed-effects components in (5.3) yields a relative risk multiplier for each municipality week, driven purely by observed climate and environmental conditions:

$$\widehat{\mu}_{it} = \exp\left\{\log(\text{pop}_{it}) + \beta_0 + [z_{\text{temp_}\ell 1}]_{it}\,\widehat{\beta}_1 + [z_{\text{precip_}\ell 1}]_{it}\,\widehat{\beta}_2 + [z_{\text{evap_}\ell 1}]_{it}\,\widehat{\beta}_3 + [z_{\text{elev}}]_{it}\,\widehat{\beta}_4\right\}.$$

This is attractive as a first-pass early-warning tool precisely because it requires no case history, making it usable even for municipalities with little or no recorded dengue data. In practice, municipality weeks could be ranked by this score and the top decile or quartile flagged as elevated risk for the coming week(s), using whichever lag the fixed-effects model specifies: one week for the GLM and four weeks for BYM2. The latter offers a longer lead time for intervention.

To illustrate this, we consider two municipalities identical in every other respect, differing only in evaporation: municipality j has evaporation one standard deviation above the mean, while municipality k has evaporation one standard deviation below it (resulting in a two-unit difference between them). Since, for the "GLM + Poisson + lag1" model, the IRR for evaporation is 0.6529 ($\widehat{\beta}_3 = -0.4264$; see Table 1), each one-unit increase multiplies expected incidence by 0.6529, so a two-unit difference compounds this to $0.6529^2 \approx 0.426$. This is because

$$\frac{\widehat{\mu}_{jt}}{\widehat{\mu}_{kt}} \approx \frac{\exp(1 \times \widehat{\beta}_3)}{\exp(-1 \times \widehat{\beta}_3)} = \exp(2\widehat{\beta}_3) = \left[\exp(\widehat{\beta}_3)\right]^2 = [\text{IRR}]^2 \approx 0.426.$$

Then municipality k, with more standing water retained (inferred from its lower evaporation), would be assigned roughly $\widehat{\mu}_{kt}/\widehat{\mu}_{jt} \approx 1/0.426 \approx 2.3$ times the expected dengue incidence of municipality j, based on this single covariate alone, without either municipality needing any recorded case history for the comparison to be made.

Evaporation stands out as the strongest multiplicative fixed effect in both models (IRRs 0.6529 and 0.5255), which raises the question of whether it is acting as a proxy for humidity or standing-water availability, the conditions that support mosquito breeding; if so, it may be the single most actionable early warning variable in the set. Elevation, being static, plays a different role: rather than serving as a dynamic warning signal, it is better used as a baseline stratification variable to define which municipalities are structurally higher or lower risk a priori, reserving the time-varying covariates for the week-to-week signal within that baseline stratification.

It is worth noting that, although fixed effects can capture important and meaningful information about changes in the risk of dengue cases, in some models, they may not explain most of the variation in the data. For instance, in the "GLM Poisson + municipality iid, lag 1" model, the municipal random intercept can carry even more weight than any single fixed effect in shaping a municipality's realized risk. Consider two municipalities, j and k, with identical covariate profiles (same temperature, precipitation, evaporation, and elevation, and hence the same fixed-effects risk score) but different unexplained baseline risk, captured by their municipal random intercepts. If municipality j's random intercept is one standard deviation above the municipal mean and municipality k's is one standard deviation below it, their expected incidence would differ by a factor of $\exp(2 \times 1.8835) \approx 6.5765^2 \approx 43.3$ (see Table 2). Holding all covariates fixed, municipality j would be expected to report roughly 43 times as many cases as municipality k, purely due to unexplained local heterogeneity, such as vector control effectiveness, water infrastructure, or historical endemicity; not captured by the four climate and elevation covariates. Even a one-standard-deviation gap alone, $\exp(1.8835) \approx 6.5765$, is enough to dwarf the roughly 2.3-fold difference between municipalities attributable to evaporation alone in the example above, underscoring how much of the realized risk differential between municipalities this unexplained component can account for.

A model built only from fixed effects, with no spatial structure, tends to under-represent municipality-specific baseline risk that the observed covariates do not explain, unobserved variables such as local vector control practices, water infrastructure, population density, or prior outbreak history. As the random-effects example above illustrates concretely, this is precisely why the GLM required such a large municipal random-intercept variance (3.5476, SD 1.8835 on the log scale): the fixed effects alone leave substantial unexplained heterogeneity, and a screening tool based on them alone will systematically miss municipalities that are structurally high-risk for reasons the climate covariates do not capture.

5.2. Local scale models (LSMs)

Although dengue transmission is distributed across much of Mexico, its spatial burden remains markedly heterogeneous. States such as Guerrero, Veracruz, and Oaxaca have long experienced recurrent transmission associated with warm climates, coastal or tropical environments, and favorable conditions for *Aedes aegypti* persistence [10]. In Veracruz, ecological studies have shown that dengue cases tend to concentrate in a limited number of recurrent localities that account for a substantial proportion of transmission, highlighting the importance of persistent hotspots [43]. More recently, national

spatial analyses have confirmed that dengue incidence in Mexico is far from randomly distributed and instead exhibits marked spatial clustering and evolving geographic patterns, with persistent activity in southern and Pacific regions, including Guerrero and Oaxaca, together with increasing importance of western and urbanized regions such as Jalisco [44]. This contrast between historically persistent transmission settings and more recent urban expansion underscores the value of examining municipal-level dynamics in locations such as Acapulco, Veracruz, Oaxaca, and Guadalajara, which represent distinct epidemiological and ecological contexts for dengue transmission. Such heterogeneity motivates the use of local modeling approaches designed to complement national analyses and better characterize regional transmission patterns.

While the national INLA model leverages full-municipality-week observations in Mexico to efficiently estimate global spatial and temporal structures, local models offer distinct and complementary advantages. First, by focusing on a single municipality and its immediate neighbors, we reduce the dimensionality of the random effects structure, transforming a computationally challenging spatial model into a manageable hierarchical model. This reduction alleviates MCMC's main limitation (poor scalability to large numbers of latent variables) while retaining its central advantage: exact posterior inference in complex, non-standard models. This is in contrast to INLA's approximations, which may perform poorly when hyperparameter posteriors are skewed or multi-modal.

Second, a local modeling strategy aligns well with the epidemiological reality of dengue transmission, which is often driven by highly localized factors: human mobility between neighboring municipalities, shared vector habitats, and microclimatic conditions that vary more within a country than across national boundaries. By modeling one focal municipality with its neighbors, we can identify and incorporate the most important covariate data that relate to the local dynamic.

The national models identified broad climatic patterns associated with dengue incidence; however, they also motivated a finer-scale analysis to determine whether these relationships remained consistent across municipalities. Municipality-level analyses revealed substantially greater heterogeneity. Rather than a uniform climatic pattern, the importance of individual predictors varied across regions, reflecting differences in local transmission dynamics.

We first fitted a saturated model including elevation, evaporation, temperature, and precipitation predictors, each lagged up to four weeks ($l = 0, \ldots, 4$). Posterior credible intervals revealed distinct sets of significant predictors for each municipality. Reduced models were then fitted using only these significant predictors.

Table S1 summarizes the diagnostics of several schemes utilized to apply brm and our local modeling to the study areas; highlighted rows in Table 4 correspond to the best diagnostic outcomes.

- **Acapulco:** Diagnostics demonstrate that this municipality can be explained robustly under either the negative binomial or Poisson family. Median ESS values are consistently high (> 2300), Rhats remain close to 1.01, and divergences are negligible. These results indicate that Acapulco's dynamics are well-captured by both distributional families, underscoring the stability of our specification in this case.
- **Veracruz:** The negative binomial specification shows acceptable diagnostics under the basic model setup described at Section 4.2. ESS values are in the thousands, Rhats for fixed and random effects remain close to 1.01 (except for the AR component, which is close to 1.02), and divergences are modest. This suggests that Veracruz can be explained appropriately without requiring extensive prior calibration.

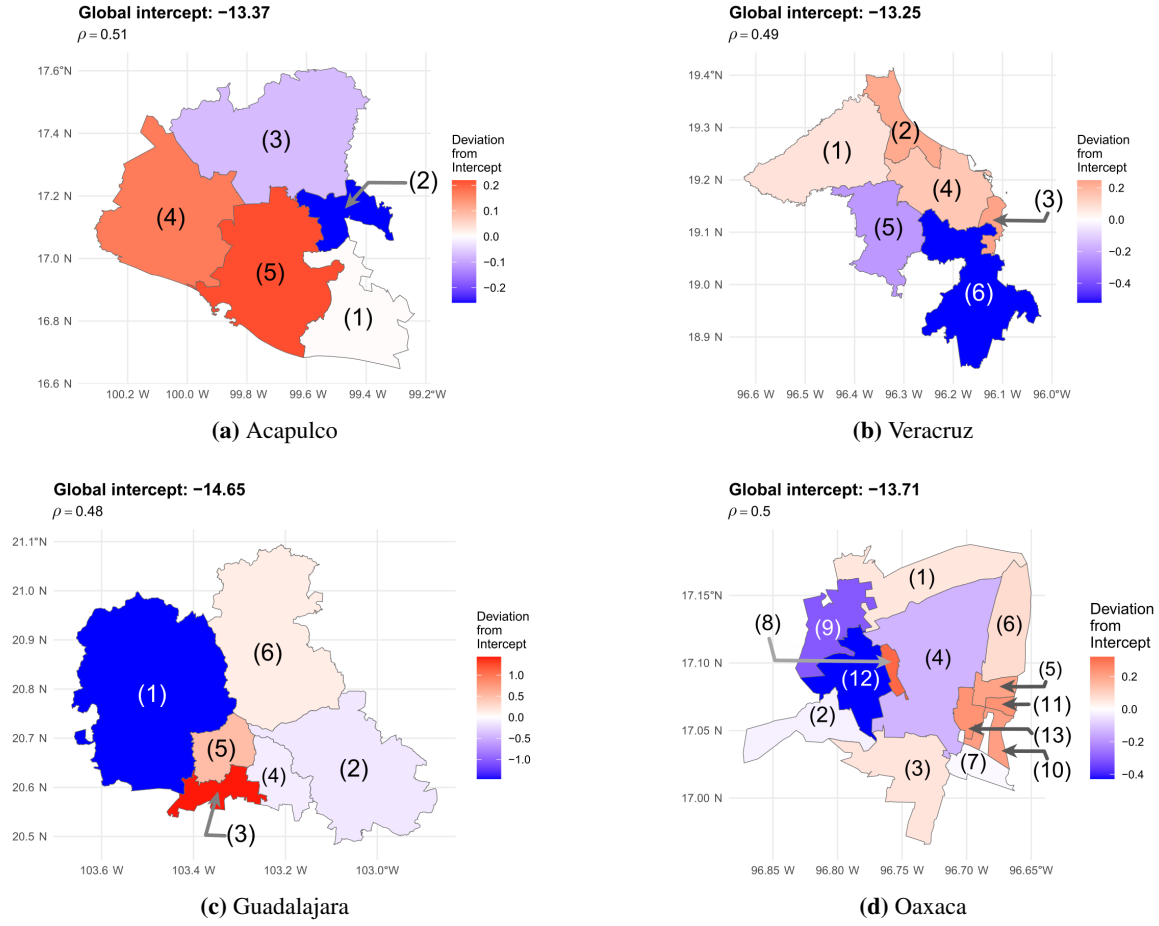
- **Guadalajara:** In contrast, Guadalajara presents the greatest challenge. Initial runs showed poor mixing, with median ESS below 20 and fixed-effect Rhats exceeding 2.5. Random-effect Rhats also reached 1.6–1.8, and divergences were non-negligible. To address this, we experimented with calibrated priors for the random effects of our model and robust posterior geometry (forced by the parameter `max_treedepth` of the brm function). The highlighted row in Table 1 demonstrates that these adjustments substantially improved diagnostics: divergences dropped to zero, ESS increased by orders of magnitude, and Rhats fell into acceptable ranges; although, this appropriate mixing was achieved by removing the AR component from the model. All in all, Guadalajara remains the most difficult municipality to achieve reliable convergence, requiring more careful tuning than the other regions.
- **Oaxaca:** Initial diagnostic checks revealed notable convergence difficulties under the Poisson family, with a divergence rate of about 3.5% and Rhat values for fixed effects reaching up to 2.006. Although the median ESS was moderate (≈ 83), the posterior geometry proved too rigid, leading to unstable estimates. Transitioning to the negative binomial family with calibrated priors and a more robust posterior geometry (similar to the strategy implemented for Guadalajara) effectively resolved these issues (see the highlighted row at the bottom of Table 1): Rhats stabilized around 1.0 and the effective sample size increased dramatically, indicating adequate chain mixing. This appropriate mixing was achieved by discarding the effect of the trend estimate for the first semester of 2018, as this parameter showed a maximum Rhat (fixed) ≈ 2.037.

Table 4. Diagnostic evaluation of brm in the study areas. Rhat (random) reports the maximum Rhat of the terms involved in the component (Municipality: u_i and v_y; CAR: ρ and σ_u; AR: ϕ_1, ϕ_2, and σ_T). The model Guadalajara^{cp,rp,*} was obtained through calibrated priors for the random effects, a robust posterior geometry, and without an AR component. For Oaxaca^{cp,rp,*}, the calculation of maximum Rhat (fixed) excluded the trend estimate of the first semester of 2018, as this parameter showed poor convergence.

		% divergent	ESS			Rhat (fixed)			Rhat (random)		
Family	Area	chains	min	median	max	min	median	max	Municipality	CAR	AR
Negative binomial											
	Acapulco	0.519	203.716	2354.326	6280.596	1.001	1.004	1.012	1.005	1.009	1.004
	Guadalajara	0.150	2.121	15.007	1156.932	1.170	1.635	2.641	1.470	1.625	1.822
	Oaxaca	7.787	2.406	110.358	641.888	1.038	1.104	1.967	1.216	1.124	1.235
	Veracruz	2.569	130.117	1214.784	7253.162	1.002	1.010	1.025	1.010	1.012	1.023
Poisson											
	Acapulco	1.456	112.517	2508.926	4056.298	1.001	1.003	1.037	1.006	1.016	1.016
	Guadalajara	0.600	2.270	15.212	82.804	1.155	1.612	2.560	2.478	1.908	1.963
	Oaxaca	3.456	2.417	83.210	278.175	1.022	1.143	2.006	1.088	1.685	1.685
	Veracruz	1.413	2.519	36.356	831.980	1.059	1.178	1.518	1.218	1.475	1.475
Poisson (calibrated priors, robust posterior)											
	Guadalajara^{cp}	0.000	3.220	196.860	1311.104	1.006	1.084	1.521	1.117	1.096	1.096
	Guadalajara^{cp,rp}	0.000	2.001	50.696	40,535.648	1.000	1.021	1.720	1.009	1.004	1.734
	Guadalajara^{cp,rp,*}	0.000	1827.875	24,882.753	34,920.726	1.000	1.000	1.001	1.000	1.001	NA
Negative binomial (calibrated priors, robust posterior)											
	Oaxaca^{cp,rp,*}	1.300	2.828	33,120.909	42,053.399	1	1	1.001	1.001	1.003	1.001

Despite improved convergence, predictive metrics favored the saturated specification. WAIC val-

ues were consistently lower for the saturated model (12,978.4, 47,865.5, 6307.3, and 21,414.2 for Acapulco, Guadalajara, Oaxaca, and Veracruz, respectively) compared to the reduced alternatives (25,144.5, 343,644.9, 13,870.5, and 61,720.3). Taken together, these results indicate that while the saturated model sacrifices some convergence stability, it provides substantially stronger out-of-sample predictive performance and remains the preferred specification for inference. For completeness, we note that both Poisson and negative binomial distributions were considered, with similar results under a zero-inflated Poisson specification. Reduced municipal models were fitted using the Poisson distribution only.



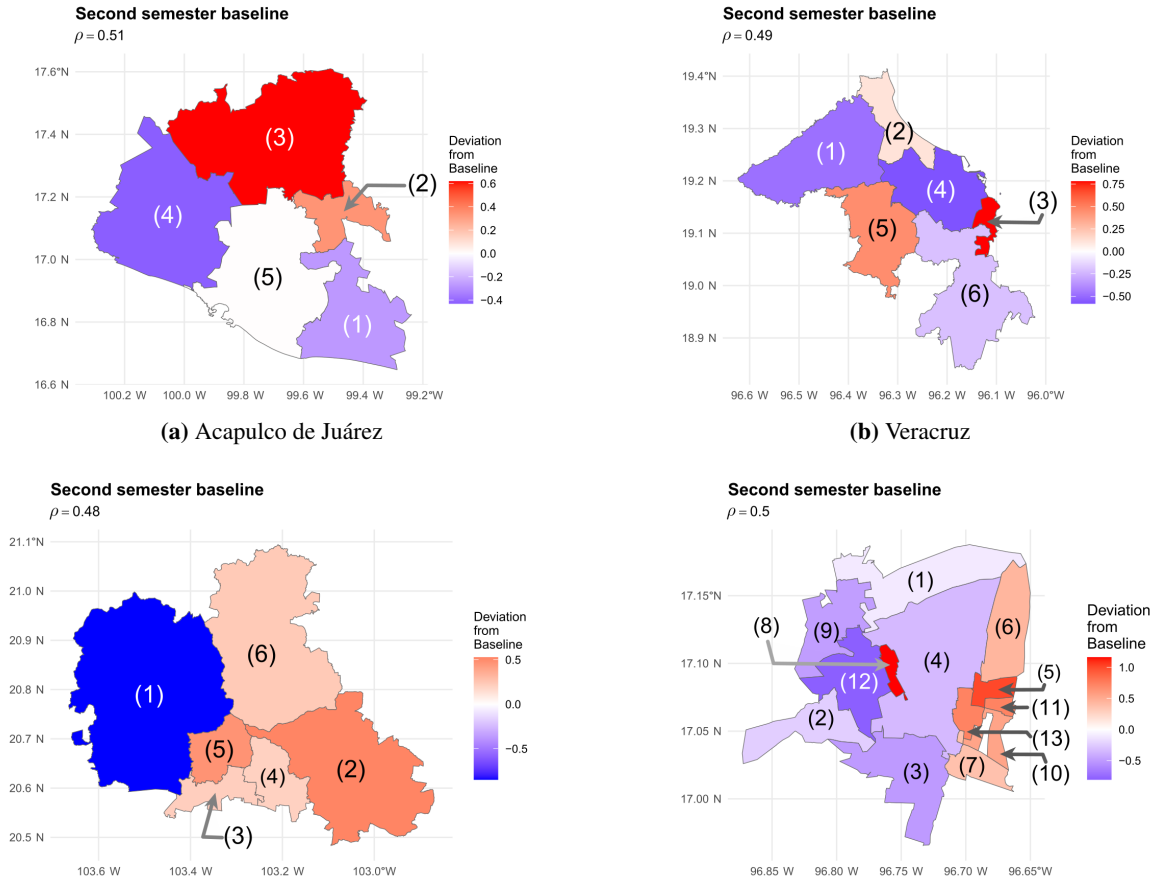
(a) Acapulco **(b)** Veracruz

(c) Guadalajara **(d)** Oaxaca

Figure 10. Municipality-specific conditional autoregressive (CAR) intercept deviations estimated under the negative binomial (Acapulco, Oaxaca, and Veracruz) and Poisson (Guadalajara) families of the local dengue models. Each subfigure corresponds to one focal metropolitan area and displays the posterior spatial deviations for its surrounding municipalities.

In Bayesian hierarchical models, the random effects represent municipality-specific characteristics: posterior deviations from the global intercept or semester baseline after accounting for fixed effects and spatial autocorrelation. These random effects (or ranef tables) are centered around zero, with positive estimates indicating municipalities where dengue incidence is elevated relative to the CAR-adjusted baseline, and negative estimates indicating suppressed incidence. To make these latent deviations

interpretable, we project them onto maps, where their magnitude and sign are visualized. Figure 10 is this spatial representation that highlights clusters of municipalities with similar deviations, turning abstract posterior estimates into epidemiologically meaningful patterns.



(a) Acapulco de Juárez

(b) Veracruz

(c) Guadalajara

(d) Oaxaca

Figure 11. Municipality-specific CAR semester effects estimated under the negative binomial (Acapulco, Oaxaca, and Veracruz) and Poisson (Guadalajara) families of the local dengue models. Semester-specific CAR random effects revealed modest deviations in Acapulco and Guadalajara, with Chilpancingo de los Bravo (3) and Zapotlanejo (2) tending positive and Zapopan (1) negative. Oaxaca displayed sharper contrasts, with San Jacinto Amilpas (8) and San Agustín Yatareni (5) strongly positive and Santa María Atzompa (12) clearly negative. Veracruz showed a mixed pattern, highlighted by Boca del Río (3) tending positive and Veracruz city (4) negative.

The posterior random effects revealed distinct spatial patterns across the study areas. In Acapulco, most municipalities clustered near zero, with Acapulco de Juárez (5) and Coyuca de Benítez (4) showing mild positive deviations and Juan R. Escudero (2) leaning negative; numbers refer to municipalities in the visualizations of Figure 10. Oaxaca displayed a similar pattern of modest heterogeneity: municipalities such as San Jacinto Amilpas (8) and Santa Lucía del Camino (11) tended positive, whereas San Lorenzo Cacaotepec (9) and Santa María Atzompa (12) leaned negative, though all estimates remained

close to zero with wide uncertainty intervals. These results suggest that both Acapulco and Oaxaca exhibit only weak municipality-specific deviations from the CAR-adjusted baseline.

By contrast, Guadalajara and Veracruz showed stronger contrasts. In Guadalajara, San Pedro Tlaquepaque (3) and Guadalajara city (5) exhibited positive deviations, while Zapopan (1) stood out with a pronounced negative effect, highlighting spatial heterogeneity within the metropolitan area. In Veracruz, Medellín de Bravo (6) consistently leaned negative, whereas Boca del Río (3) and La Antigua (2) tended positive, with Veracruz city (4) itself slightly elevated. These findings emphasize that while some regions (Acapulco, Oaxaca) display modest deviations, others (Guadalajara, Veracruz) reveal sharper contrasts in municipality-specific incidence, underscoring the importance of spatially explicit modeling.

The semester effects capture how dengue incidence shifts during the second half of the year across municipalities, after accounting for spatial autocorrelation. Positive values indicate areas where incidence tends to rise in the latter semester, while negative values mark places where incidence is suppressed. It is not easy to interpret these estimates directly, but they are more interpretable when they are projected onto maps. Figure 11 depicts these local effects, where seasonal deviations become visible as spatial gradients and clusters.

The semester-specific CAR random effects revealed distinct local patterns across the metropolitan areas. In Acapulco, most municipalities clustered near zero, with Chilpancingo de los Bravo (3) showing a clear positive deviation and Coyuca de Benítez (4) leaning negative. Guadalajara displayed a similar mix: Zapopan (1) stood out with a pronounced negative effect, while Zapotlanejo (2) and Guadalajara city (5) tended positive, highlighting heterogeneity within the metropolitan zone.

Oaxaca and Veracruz exhibited sharper contrasts. In Oaxaca, San Jacinto Amilpas (8) and San Agustín Yatareni (5) showed strong positive semester effects, whereas Santa María Atzompa (12) presented a significant negative deviation. Veracruz revealed a comparable duality, with Boca del Río (3) positively affected and Veracruz city (4) and Paso de Ovejas (1) leaning negative. These results emphasize that semester-specific deviations are modest in Acapulco and Guadalajara but more pronounced in Oaxaca and Veracruz, underscoring the importance of temporal shocks in shaping local dengue dynamics.

6. Conclusions

In this work, we analyzed the relationship between climatic variables and dengue incidence in Mexico using statistical models at two spatial scales. National- and municipality-level analyses should be viewed as complementary rather than competing approaches. National models describe broad spatial and temporal patterns of dengue incidence, whereas municipality-level analyses provide a finer description of local transmission dynamics and reveal heterogeneity that is not apparent in a nationwide analysis.

At the national scale, climatic covariates together with municipality-level random effects explained a large proportion of the observed variability in dengue incidence. In this setting, the non-spatial GLMs generally performed better than the corresponding spatial INLA models: the best-performing model overall, the GLM Poisson model, achieved a lower RMSE and a higher observed–predicted correlation than the best-performing spatial model, the BYM2 model, suggesting that the climatic variables considered in this study, together with municipality-specific heterogeneity, already account for much

of the large-scale variation in dengue incidence. This conclusion is directly supported by three complementary pieces of evidence presented in Section 5.1. First, the fixed-effect estimates in Table 1 show consistent, statistically robust associations between dengue incidence and temperature, precipitation, evaporation, and elevation in both selected models, with temperature and precipitation increasing incidence (IRR $>$ 1) and evaporation and elevation decreasing it (IRR $<$ 1). Second, the municipal random-intercept variance reported in Table 2 corresponds to an approximately 6.6-fold multiplicative difference in baseline dengue risk across municipalities, and the BYM2 mixing parameter (0.854) indicates that most of the residual, climate-unexplained variability is spatially structured together, demonstrating that persistent municipality-level heterogeneity, not captured by climate alone, is a major driver of the observed national variability. Third, the predictive validation results in Table 3 confirm that models with the heterogeneity described by the random effects and/or GLM Poisson model reproduce the observed spatiotemporal patterns of dengue substantially better than models based on climate alone. The spatial representation of the two selected predictive models presents under- or over-prediction that is not random across the country but seems to form spatially coherent clusters, pointing to specific municipalities where unmeasured local processes, e.g., outbreak intensity, surveillance heterogeneity, or vector-control activity, remain important and where climate-based predictions alone are least reliable for guiding local dengue management. In non-spatial models, the Poisson distribution consistently provided a better fit than the zero-inflated formulations, indicating that excess zeros are not a dominant feature of the national surveillance data.

The comparison among lag structures also revealed differences between the two approaches. Shorter lags, particularly one and two weeks, generally produced better predictive performance in the non-spatial models, whereas longer lags performed better in the spatial INLA models. This finding suggests that climatic effects are represented over different temporal scales depending on the modeling approach. In the non-spatial models, climatic variables appear to capture more immediate changes in dengue transmission, whereas in the spatial models, longer lags become more informative after spatial dependence has been taken into account.

The explored NSMs have the limitation of assuming a linear (or link-scale linear) relationship between climatic covariates and dengue risk, and of evaluating only one lag at a time rather than distributed or cumulative lag structures. As a result, they may not fully capture nonlinear effects such as temperature thresholds or rainfall saturation, nor the cumulative influence of climatic exposure across multiple weeks. However, given the limited prior statistical modeling work available for dengue prediction at this national scale, and because fitting the full set of candidate models already required considerable computational time, underscoring the practical cost of extending the framework further, our intention is to put these models forward as a transparent baseline: one that identifies important dengue covariates and their most relevant associations, and that supports short-term dengue prediction. A next step is to explore more general models that allow for nonlinear and threshold effects (for instance, through splines, kernel-based structures, or distributed lag nonlinear models (DLNMs)), as well as alternative lag specifications for both dependent and independent variables that enable longer-term predictions. Incorporating other potentially important covariates (such as socioeconomic conditions, surveillance quality, vector control activities, population movement, and circulating dengue serotypes) at the municipality level is also highly desirable; however, as this information is often unavailable at this spatial resolution, future work should explore suitable proxies, composite environmental or socioeconomic indicators, and alternative modeling strategies, together with variable-selection approaches.

The national-level models presented here provide a basis for developing early warning tools that could identify regions at higher risk of dengue transmission and support timely public health interventions. However, these models need further refinement before they can reliably serve this purpose. In their current form, a large share of the variability is absorbed by the random effects, which capture unexplained spatial and temporal heterogeneity but offer limited insight into their underlying drivers. A more detailed specification would allow a more precise description of spatial variation and could incorporate covariates that may be particularly relevant in certain regions, such as local climatic, environmental, or socioeconomic conditions, rather than leaving their influence implicitly accounted for by the random effects. Such region-specific extensions would improve both the interpretability of the models and their usefulness for targeted surveillance.

The municipality-level analyses complemented the national results by revealing substantial local heterogeneity. Although the same climatic variables were considered in all study areas, their relative importance differed among municipalities, reflecting differences in local transmission dynamics. The municipality-specific random effects and seasonal effects also revealed spatial patterns that were not explained by the climatic covariates alone. These findings suggest that additional information, such as human mobility, socioeconomic conditions, demographic characteristics, land-use characteristics, or vector-control activities, may help explain the remaining variability in dengue transmission. More importantly, they indicate that the relationship between climatic variables and dengue incidence depends on the spatial scale of analysis, emphasizing the importance of selecting an appropriate spatial resolution when studying dengue transmission.

It is also important to note that the saturated local models, which we retained for inference due to their superior out-of-sample predictive performance (lower WAIC; see Section 5.2), showed heterogeneous convergence across sites, with median $\hat{R}$ values ranging from 1.0033 (Acapulco) to 1.612 (Guadalajara). This indicates that posterior estimates for some municipalities, particularly Guadalajara, should be interpreted with additional caution, and reinforces the need to frame local-scale findings as indicative of regional heterogeneity rather than as precise, fully converged point estimates.

One limitation of the present study is that the analyses only considered climatic and geographic variables as explanatory covariates. Consequently, all reported relationships between climatic covariates and dengue incidence should be interpreted as statistical associations rather than causal effects. Several important factors that are known to influence dengue transmission were not available for this analysis, including surveillance quality and reporting completeness, vector-control interventions, human population mobility, and the circulation of different dengue serotypes, all of which can modulate incidence independently of climate and may partly explain the residual municipal and spatial heterogeneity identified in both the national and local models. Future work will focus on extending this framework by incorporating these variables, where data become available, and by evaluating its application to other vector-borne diseases.

Use of AI tools declaration

The authors declare they have not used Artificial Intelligence (AI) tools in the creation of this article.

Acknowledgments

M. Núñez-López acknowledges support from the Secretaría de Ciencia, Humanidades, Tecnología e Innovación grant CBF-2025-G-57 and from Asociación Mexicana de Cultura, A.C. She also gratefully acknowledges the University of Castilla-La Mancha for its hospitality and research facilities, where part of this work was carried out.

Conflict of interest

The authors declare there is no conflict of interest.

References

1. S. Bhatt, P. W. Gething, O. J. Brady, J. P. Messina, A. W. Farlow, C. L. Moyes, et al., The global distribution and burden of dengue, *Nature*, **496** (2013), 504–507. https://doi.org/10.1038/nature12060
2. World Health Organization, *Dengue and Severe Dengue*, 2025. Available from: https://www.who.int/health-topics/dengue-and-severe-dengue#tab=tab_1.
3. E. A. Mordecai, J. M. Cohen, M. V. Evans, P. Gudapati, L. R. Johnson, C. A. Lippi, et al., Detecting the impact of temperature on transmission of Zika, dengue, and chikungunya using mechanistic models, *PLoS Negl. Trop. Dis.*, **11** (2017), e0005568. https://doi.org/10.1371/journal.pntd.0005568
4. O. J. Brady, M. A. Johansson, C. A. Guerra, S. Bhatt, N. Golding, D. M. Pigott, et al., Modelling adult *Aedes Aegypti* and *Aedes Albopictus* survival at different temperatures, *Parasites Vectors*, **6** (2014), 351. https://doi.org/10.1186/1756-3305-6-351
5. L. Feng, C. Caminade, S. A. Müller, E. A. Mordecai, T. K. Yamana, M. U. G. Kraemer, et al., Temperature-driven dengue transmission in a changing climate: Patterns, trends, and future projections, *GeoHealth*, **8** (2024), e2024GH001059. https://doi.org/10.1029/2024GH001059
6. A. G. Lemma, G. T. Tilahun, B. T. Bekele, Modeling the impact of climate change on dengue transmission dynamics in Dire Dawa, Afar, and Somali, Ethiopia: An African regional perspective, *Sci. Rep.*, **15** (2025), 33979. https://doi.org/10.1038/s41598-025-10648-0
7. M. A. Johansson, F. Dominici, G. E. Glass, Local and global effects of climate on dengue transmission in Puerto Rico, *PLoS Negl. Trop. Dis.*, **3** (2009), e382. https://doi.org/10.1371/journal.pntd.0000382
8. Z. Xu, H. Bambrick, L. Yakob, G. Devine, J. Lu, F. D. Frentiu, et al., Spatiotemporal patterns and climatic drivers of severe dengue in Thailand, *Sci. Total Environ.*, **656** (2019), 889–901. https://doi.org/10.1016/j.scitotenv.2018.11.395
9. G. Li, P. Lu, P. Weinstein, A. Urban, S. Tong, N. Ryti, et al., The burden of El Niño–Southern Oscillation-related dengue attributable to anthropogenic climate change: A multicountry modelling study, *Lancet Planet. Heath*, **10** (2026), 101454. https://doi.org/10.1016/j.lanplh.2026.101454

10. M. Hurtado-Díaz, H. Riojas-Rodríguez, S. J. Rothenberg, H. Gomez-Dantés, E. Cifuentes, Impact of climate variability on the incidence of dengue in Mexico, *Trop. Med. Int. Health*, **12** (2007), 1327–1337. https://doi.org/10.1111/j.1365-3156.2007.01930.x

11. M. Gharbi, P. Quenel, J. Gustave, S. Cassadou, G. L. Ruche, L. Girdary, et al., Time series analysis of dengue incidence in Guadeloupe, French West Indies: Forecasting models using climate variables as predictors, *BMC Infect. Dis.*, **11** (2011), 166. https://doi.org/10.1186/1471-2334-11-166

12. O. J. Brady, P. W. Gething, S. Bhatt, J. P. Messina, J. S. Brownstein, A. G. Hoen, et al., Refining the global spatial limits of dengue virus transmission by evidence-based consensus, *PLoS Negl. Trop. Dis.*, **6** (2012), e1760. https://doi.org/10.1371/journal.pntd.0001760

13. J. P. Messina, O. J. Brady, N. Golding, M. U. G. Kraemer, G. R. W. Wint, S. E. Ray, et al., The current and future global distribution and population at risk of dengue, *Nat. Microbiol.*, **4** (2019), 1508–1515. https://doi.org/10.1038/s41564-019-0476-8

14. M. H. Bukhari, M. Y. Shad, U. S. D. T. Nguyen, C. J. A. Treviño, W. Jung, W. U. Bajwa, et al., A Bayesian spatiotemporal approach to modelling arboviral diseases in Mexico, *Trans. R. Soc. Trop. Med. Hyg.*, **117** (2023), 867–874. https://doi.org/10.1093/trstmh/trad064

15. R. Lowe, C. Barcellos, C. A. S. Coelho, T. C. Bailey, G. E. Coelho, R. Graham, et al., Dengue outlook for the World Cup in Brazil: An early warning model framework driven by real-time seasonal climate forecasts, *Lancet Infect. Dis.*, **14** (2014), 619–626. https://doi.org/10.1016/S1473-3099(14)70781-9

16. C. Mills, C. A. Donnelly, Climate-based modelling and forecasting of dengue in three endemic departments of Peru, *PLoS Negl. Trop. Dis.*, **18** (2024), e0012596. https://doi.org/10.1371/journal.pntd.0012596

17. S. Wu, A. G. Meyer, L. Clemente, L. M. Stolerman, F. Lu, A. Majumder, et al., Ensemble approaches for short-term dengue fever forecasts, *Proc. Natl. Acad. Sci. U.S.A.*, **122** (2025), e2422335122. https://doi.org/10.1073/pnas.2422335122

18. X. Chen, P. Moraga, Assessing dengue forecasting methods: A comparative study of statistical models and machine learning techniques in Rio de Janeiro, Brazil, *Trop. Med. Health*, **53** (2025), 52. https://doi.org/10.1186/s41182-025-00723-7

19. J. M. Caldwell, A. D. LaBeaud, E. F. Lambin, A. M. Stewart-Ibarra, B. A. Ndenga, F. M. Mutuku, et al., Climate predicts geographic and temporal variation in mosquito-borne disease dynamics on two continents, *Nat. Commun.*, **12** (2021), 1233. https://doi.org/10.1038/s41467-021-21496-7

20. Y. Li, Q. Dou, Y. Lu, H. Xiang, X. Yu, S. Liu, Effects of ambient temperature and precipitation on the risk of dengue fever: A systematic review and updated meta-analysis, *Environ. Res.*, **191** (2020), 110043. https://doi.org/10.1016/j.envres.2020.110043

21. CONAPO, *Población a Mitad de Año por Municipio y Grupos Quinquenales de Edad (1990–2040)*, 2025. Available from: https://www.datos.gob.mx/dataset/proyecciones-de-poblacion/resource/3c3092be-583e-4490-8c23-67ef9a64b198.

22. INEGI, *Marco de Referencia ITRF en México y su Relación con WGS84 y NAD27*, 2019. Available from: https://www.inegi.org.mx/contenidos/temas/gnss/doc/702825109226.pdf.

23. J. Muñoz-Sabater, E. Dutra, A. Agustí-Panareda, A. Albergel, G. Arduini, G. Balsamo, et al., ERA5-Land: A state-of-the-art global reanalysis dataset for land applications, *Earth Syst. Sci. Data*, **13** (2021), 4349–4383. https://doi.org/10.5194/essd-13-4349-2021

24. European Centre for Medium-Range Weather Forecasts (ECMWF), *European Centre for Medium-Range Weather Forecasts*, 2025. Available from: https://www.ecmwf.int/.

25. C. J. Willmott, K. Matsuura, Smart interpolation of annually averaged air temperature in the United States, *J. Appl. Meteorol. Climatol.*, **34** (1995), 2577–2586. https://doi.org/10.1175/1520-0450(1995)034<2577:SIOAAA>2.0.CO;2

26. P. Zhao, Z. He, A first evaluation of ERA5-land reanalysis temperature product over the Chinese Qilian mountains, *Front. Earth Sci.*, **10** (2022), 907730. https://doi.org/10.3389/feart.2022.907730

27. R. J. Hijmans, Cross-validation of species distribution models: Removing spatial sorting bias and calibration with a null model, *Ecology*, **93** (2012), 679–688. https://doi.org/10.1890/11-0826.1

28. J. Zou, N. Lu, H. Jiang, J. Qin, L. Yao, Y. Xin, F. Su, Performance of air temperature from ERA5-Land reanalysis in coastal urban agglomeration of Southeast China, *Sci. Total Environ.*, **828** (2022), 154459. https://doi.org/10.1016/j.scitotenv.2022.154459

29. Y. R. Wang, D. O. Hessen, B. H. Samset, F. Stordal, Evaluating global and regional land warming trends in the past decades with both MODIS and ERA5-Land land surface temperature data, *Remote Sens. Environ.*, **280** (2022), 113181. https://doi.org/10.1016/j.rse.2022.113181

30. N. Gorelick, M. Hancher, M. Dixon, S. Ilyushchenko, D. Thau, R. Moore, Google Earth Engine: Planetary-scale geospatial analysis for everyone, *Remote Sens. Environ.*, **202** (2017), 18–27. https://doi.org/10.1016/j.rse.2017.06.031

31. M. Chan, M. A. Johansson, The incubation periods of dengue viruses, *PLoS One*, **7** (2012), e50972. https://doi.org/10.1371/journal.pone.0050972

32. J. A. Nelder, R. W. M. Wedderburn, Generalized linear models, *J. R. Stat. Soc. A*, **135** (1972), 370–384. https://doi.org/10.2307/2344614

33. C. E. McCulloch, J. M. Neuhaus, Generalized linear mixed models: Estimation and inference, *SAGE Handb. Multilevel Model.*, **2013** (2013), 271–286.

34. P. McCullagh, J. A. Nelder, *Generalized Linear Models*, 2nd Edition, Chapman and Hall, London, 1989.

35. A. C. Cameron, P. K. Trivedi, *Regression Analysis of Count Data*, 2nd Edition, Cambridge University Press, Cambridge, 2013.

36. J. M. Hilbe, *Negative Binomial Regression*, 2nd Edition, Cambridge University Press, Cambridge, 2011.

37. H. Rue, S. Martino, N. Chopin, Approximate Bayesian inference for latent Gaussian models by using integrated nested Laplace approximations, *J. R. Stat. Soc. B*, **71** (2009), 319–392. https://doi.org/10.1111/j.1467-9868.2008.00700.x

38. F. Lindgren, H. Rue, J. Lindström, An explicit link between Gaussian fields and Gaussian Markov random fields: the stochastic partial differential equation approach, *J. R. Stat. Soc. B*, **73** (2011), 423–498. https://doi.org/10.1111/j.1467-9868.2011.00777.x

39. J. Besag, J. York, A. Mollié, Bayesian image restoration, with two applications in spatial statistics, *Ann. Inst. Stat. Math.*, **43** (1991), 1–20. https://doi.org/10.1007/BF00116466

40. P. C. Bürkner, brms: An R package for Bayesian multilevel models using Stan, *J. Stat. Software*, **80** (2017), 1–28. https://doi.org/10.18637/jss.v080.i01

41. P. C. Bürkner, Advanced Bayesian multilevel modeling with the R package brms, *R J.*, **10** (2018), 395–411. https://doi.org/10.32614/RJ-2018-017

42. P. C. Bürkner, Bayesian item response modeling in R with brms and Stan, *J. Stat. Software*, **100** (2021), 1–54. https://doi.org/10.18637/jss.v100.i05

43. J. Escobar-Mesa, H. Gomez-Dantes, Dengue fever transmission in Veracruz, Mexico: An ecological approach to disease control, *Salud Publ. Mex.*, **45** (2003), 43–53.

44. O. Mendoza-Cano, R. Danis-Lozano, X. Trujillo, M. Huerta, M. Rios-Silva, A. Lugo-Radillo, et al., Spatial patterns and clustering of dengue incidence in Mexico: Analysis of Moran's index across 2471 municipalities from 2022 to 2024, *PLoS One*, **20** (2025), e0324754. https://doi.org/10.1371/journal.pone.0324754



AIMS Press

© 2026 the Author(s), licensee AIMS Press. This is an open access article distributed under the terms of the Creative Commons Attribution License (https://creativecommons.org/licenses/by/4.0)